NANO · MICRO small
www.small-journal.com

Recent Progress of Carbon Dots for Air Pollutants Detection and Photocatalytic Removal: Synthesis, Modifications, and Applications

Jungang Zhao, Caiting Li, Xueyu Du, Youcai Zhu, Shanhong Li, Xuan Liu, Caixia Liang, Qi Yu, Le Huang, and Kuang Yang*

Rapid industrialization has inevitably led to serious air pollution problems, thus it is urgent to develop detection and treatment technologies for qualitative and quantitative analysis and efficient removal of harmful pollutants. Notably, the employment of functional nanomaterials, in sensing and photocatalytic technologies, is promising to achieve efficient in situ detection and removal of gaseous pollutants. Among them, carbon dots (CDs) have shown significant potential due to their superior properties, such as controllable structures, easy surface modification, adjustable energy band, and excellent electron-transfer capacities. Moreover, their environmentally friendly preparation and efficient capture of solar energy provide a green option for sustainably addressing environmental problems. Here, recent advances in the rational design of CDs-based sensors and photocatalysts are highlighted. An overview of their applications in air pollutants detection and photocatalytic removal is presented, especially the diverse sensing and photocatalytic mechanisms of CDs are discussed. Finally, the challenges and perspectives are also provided, emphasizing the importance of synthetic mechanism investigation and rational design of structures.

1. Introduction

As the world's industrial processes continue to advance, environmental issues have drawn growing attention. In particular, the harmful and toxic air pollutants are causing global concerns. Various types of toxic gases such as nitrogen oxides (NO_x), sulfur dioxide (SO_2), and volatile organic compounds (VOCs, including alcohols, aromatics, aldehydes, and halocarbons) are derived from industrial and mobiles sources.[1,2] Moreover, some VOCs and odorous gases (NH_3, H_2S, etc.) are emitted from the indoor environment and human metabolism as well as domestic waste corruption.[3,4] The harmful gases released into the air can threaten human health as the cause of respiratory diseases, headaches, and allergies.[5,6] Long-term exposure to high levels of air-polluted environment can even induce cancer.[7] Chromatography and its derivatization techniques are the most frequently used methods for the determination of air pollutants. However, chromatography and its ancillary equipment are expensive and require complex pre-treatment processes and long-time analysis. Further, most conventional systems are too large to employ for on-site detection. It is extremely essential to develop advanced sensing and treatment techniques with advantages of excellent sensitivity, rapid detection, high purification efficiency, and ease operation for air pollutants monitoring and removal.

In general, the highly sensitive detection of analytes/contaminants in sensors depends heavily on the sensing signals generated by the variations in optical, electrical, or photophysical properties of the sensing materials when they interact with the analytes. Therefore, the choice and design of the sensing substrates used in the detection platform are critical to the performance of the sensors. For the past few years, the nanomaterials, such as carbon-based nanomaterials, metal-organic frameworks, and coordination polymers, have provided powerful platforms to achieve high sensitivity and selectivity detection of pollutants.[8–10] However, there are still some factors that limit their application, such as high costs and the participation of toxic reagents during the synthesis process.[11,12]

CDs are a general term for a class of carbon nanodots (CNDs), including graphene quantum dots, CNDs, polymer dots (PDs), and carbon quantum dots.[13] They can be prepared from inexpensive and easily available reagents and facile synthesis methods.[9] Moreover, the morphology and composition of CDs are controlled by different synthesis routes, precursors, and modification methods, which in turn lead to various

J. Zhao, C. Li, X. Du, Y. Zhu, S. Li, X. Liu, C. Liang, Q. Yu, L. Huang, K. Yang
College of Environmental Science and Engineering
Hunan University
Changsha 410082, P. R. China
E-mail: ctli@hnu.edu.cn
J. Zhao, C. Li, X. Du, Y. Zhu, S. Li, X. Liu, C. Liang, Q. Yu, L. Huang, K. Yang
Key Laboratory of Environmental Biology and Pollution Control (Hunan University)
Ministry of Education
Changsha 410082, P. R. China

The ORCID identification number(s) for the author(s) of this article can be found under https://doi.org/10.1002/smll.202200744.

DOI: 10.1002/smll.202200744

photoelectric and adsorption properties of CDs. Even though, they generally have similar features such as nontoxic, rich surface/edge sites, tunable photoluminescence, easily modifiable structure, superior electron mediator property, and wide-spectrum response. So they have attracted widespread attention and shown outstanding performance in the fields of sensing, biological probes, catalysis, optical imaging, energy conversion, etc.[12,14–16] A large number of studies have reported that CDs have great potential in water environmental toxic pollutants monitoring and treatment.[17–22] Saleh's group reviewed the recent advances in fluorescence detection and photocatalytic removal of metal ions, dyes, explosive nitro compounds, pesticides, and biomolecules by using biomass-and chemical-derived functionalized CDs.[16] Murilo et al. summarized the reports on the contaminant adsorption and hazardous analytes detection (including heavy metals, antibiotics, and pesticides) of CDs nanocomposites.[23] More recently, a review focused on the applications of CDs in antibiotics adsorption, membrane separation, and antimicrobial was reported by Qing's group.[24] However, there are very few reviews systematically discussing the detection and removal of air pollutants with CDs-based materials. By now, only Dolai et al. overviewed the research progress of selective and sensitive recognition of VOCs based on the fluorescence detection mechanism of CDs.[25] There are still gaps in the review on the electrochemical detection mechanism of gaseous pollutants and photocatalytic removal of air contaminants using CDs-based materials.

CDs, with active surface and superior optical electric properties, can generate interactions with different air contaminants thus producing variable photoelectronic signals, which could be used for providing more viable options to air pollutants detection. Moreover, taking advantage of the unique characteristics, such as adjustable energy band, broad-spectrum absorption, up-conversion photoluminescence, and excellent electron acceptor/donor properties, CDs can be designed as photocatalysts for air pollutants removal. Hence, this manuscript is intended to focus on the recent progress in synthesis and performance modulation of CDs, as well as their mechanisms and applications regarding air pollutants detection and photocatalytic removal, specifically including: 1) A brief introduction on the properties, preparation, and modification strategies of CDs (Section 2). 2) The classification of sensors according to the different forms of signals generated by the interaction between CDs and gaseous pollutants, and the sensing mechanism as well as examples of CDs-based sensors for air pollutants (Section 3). 3) The experimental and theoretical computational studies of CDs-modified photocatalysts for the removal of typical air pollutants including NO_x and VOCs (Section 4). 4) Some perspectives and challenges in developing and designing CDs for air pollutants detection and photocatalytic removal (Section 5). It is anticipated that this review will provide valuable guidance for future research on the improvement of the air environment.

2. Properties, Synthesis, and Modifications of Carbon Dots

CDs are regarded as valuable nanomaterials in the field of environmental monitoring and treatment due to their superior characteristics, including specific molecular adsorption, adjustable photoluminescence (PL) properties, broad solar spectrum absorption, excellent electron transfer abilities, and controllable energy band. Additionally, they can be synthesized by different preparation routes and their optical and electrochemical properties are readily tuned via the modification of morphological regulation, heteroatom doping, and surface functionalization. The specific properties, synthesis, and modification strategies will be described below in further detail.

2.1. Properties of Carbon Dots

CDs, with sizes below 10 nm, are zero-dimension spherical particles with a special kind of "core–shell" nanostructure, including nanoscale carbon cores and shells of soft materials.[26] The graphitic phase carbon and amorphous carbon coexist in CDs. The lattice spacing of 0.34 and 0.21 nm correspond to (002) and (100) crystal planes of the graphite, respectively.[27,28] The zero-dimension CDs inherently possess relatively large specific surface areas and abundant surface defects as well as functional groups, including aromatic rings, carboxyl, hydroxyl, and amino groups.[29] When the sizes of CDs are smaller than the exciton Bohr radius, the electron distribution will change significantly, exhibiting relevant size-dependent properties and quantum effects, known as quantum confinement and edge effects.[30] Meanwhile, the sizes and surface states of CDs influence their bandgap width, which is responsible for the unique optical and electrical properties, such as adjustable PL properties and variable electrical conductivity.[31]

2.1.1. Optical Properties

The PL property is one of the most prominent features of CDs, which is related to the existence of the bandgap as mentioned above.[32–34] By absorbing photons with energy higher than the bandgap, the electrons leap to the valence band from the conduction band and reach the excited state. When they restore to the base state, energy is released as photons.[35] The fluorescence intensity of CDs can be measured by the quantum yield (QY), which is the ratio of emitted photons to absorbed incident photons of the material. In other words, QY denotes the probability of the transition of a substance from the excited state to the fundamental state by radiative emission of fluorescence.[36] The PL behavior of CDs can be theoretically tailored by tuning the particle sizes, the types of edges, and surface states.[37] In general, the wavelength of the emitted light is longer than excited light due to the occurrence of energy loss in the electron excitation process. Nevertheless, the CDs' up-conversion photoluminescence property is the opposite of the phenomenon mentioned above. The unique up-conversion photoluminescence property has made CDs spectral converters that have enormous potential to utilize longer sunlight wavelengths, even the near-infrared (NIR) irradiation. However, the mechanism of PL is still ongoing debate by now. Some theories have been developed to illustrate this property, such as surface defect states, emissive traps, crosslink-improved emission effects, and quantum confinement effects.[13,38] Moreover, the PL performance of CDs can

be significantly influenced by external environmental conditions (like temperature, pH, and medium),[39–42] and the PL of CDs can be quenched by either electron donors (e.g., *N,N*-diethylaniline), or electron acceptors (e.g., 4-nitrotoluene).[43]

Optical absorption is another essential feature of CDs. CDs typically exhibit significant absorption in the ultraviolet region (200–400 nm), with tails extending into the visible range. The absorption shoulders belong to the $n \rightarrow \sigma^*$ transitions of the C—O/C—N bonds, the $n \rightarrow \pi^*$ transitions of the C = O/C = N bonds, and the $\pi \rightarrow \pi^*$ transitions of the C = C bonds.[37,44] Since the absorption spectra of CDs cover the spectral range available in the field of photocatalysis and combined with the up-conversion properties, CDs can be used as photosensitizers to extend the photoactive region when compounded with other wide bandgap photocatalysts. For instance, Li et al. prepared Cu_2O modified with CDs via a one-step ultrasonic method for CO_2 reduction.[45] Compared to pure Cu_2O, the incorporation of CDs enhanced the optical absorption and ultimately improved the photocatalytic performance.

2.1.2. Electrical Properties

CDs are composed of conjugated sp^2/sp^3 hybridized carbon and rich surface functional groups. Their electrical conductivity is highly associated with the proportion of carbon in the sp^2 hybridized state, size, and surface groups. Numerous studies have demonstrated that the excellent electron transport performance of CDs facilitates the separation of carriers and interfacial charge transfer with electrolytes, reactants, or other nanomaterials.[46,47] Ma and co-workers examined the electron transfer ability of CDs in N-CDs/Cu_2O composites.[48] Electrochemical impedance spectroscopy results of N-CDs/Cu_2O exhibited the semicircle nature and smaller Nyquist curve radius than pure Cu_2O in the high-frequency region, indicating that N-CDs/Cu_2O had superior charge transfer capabilities than pure Cu_2O cubes. Fei et al. fabricated B,N-doped CDs/graphene hybrid nanoplatelets and found the optimized samples exhibited excellent electrocatalytic ability with a higher positive onset potential than commercial Pt/C and a larger current density.[49]

Moreover, the electrical properties of CDs can be modulated by heteroatom doping, functional groups regulation, and geometry optimization.[46,50] Wu's group found that N-CDs doped with Cu atom could further improve electron-accepting/donating performance and conductivity attributed to Cu,N-CDs charge-transfer absorption.[51] Feng et al. investigated the effect of the position of oxygen-containing functional groups on the CDs' electrical properties.[52] It was observed that these oxygen-containing groups at the edges of CDs had little effect on such properties, while modifications on the basal surface caused larger impacts. In addition, CDs have been reported to present changes in conductivity when combined with other specific materials.[31] Therefore, CDs can provide platforms for the applications of photo/electrocatalysis and conductive sensing.[53–55]

2.1.3. Electrochemical Properties

A large number of surface functional groups, abundant edge sites, and variable bandgap endow CDs with excellent electrochemical and catalytic properties.[50,56] Reportedly, CDs can act as multivalent redox species and can be tuned by defect construction, surface modification, and elemental doping.[50,57] Furthermore, due to their low oxidation potential and affinity for positively charged ions, CDs are regarded as effective reducing agents for noble metal ions with high reduction potential, such as Au^{3+} and Ag^{+}.[58,59] Especially, photoexcited CDs show outstanding electron-donating ability, leading to fast reduction and nucleation of metal ions, which is favorable to the treatment of heavy metal ions. As an example, CDs obtained from microcrystalline cellulose reached a complete reduction of 20 ppm Cr (VI) to Cr (III) under 120 min sunlight illumination.[60]

2.1.4. Molecule Adsorption Properties

The specific functional groups and carbon sp^2 conjugate electron structure enable CDs to interact with small molecules through π–π and electrophilic interaction of chemical groups.[46] Therefore, the adsorption performance of CDs can be regulated by modulating their surface chemical states and type of functional groups. The superior molecule adsorption property of CDs facilitates the recognition and enrichment of analytes, thus exhibiting excellent performance in contaminants detection and environmental catalysis.

2.2. Synthesis of Carbon Dots

2.2.1. Top-down

There are two main strategies for synthesizing CDs including "top-down" and "bottom-up" methods, which employ macroscopic carbon sources and small molecules as precursors, respectively.[12,61,62] In the top-down method, CDs are prepared by breaking more extensive carbon-based materials (graphite, carbon black, graphene oxide, etc.) into quantum-sized particles under harsh synthetic conditions via chemical oxidation or arc-discharging, laser ablation, acidic exfoliation.[61] The first discovery of CDs was reported by Xu and co-authors in 2004.[63] They obtained the fluorescent CDs during purification of single-walled carbon nanotubes (SWCNTs) synthesized via arc-discharging soot. Afterward, Mohanty's group achieved controllable preparation of CDs with different shapes (square, rectangle, and triangle) and dimensions.[64] The synthesis process includes nanoscale-cutting of graphite into nano blocks and followed exfoliation, just as shown in **Figure 1**a. In another report, Peng's group utilized carbon fibers to prepare CDs via acid etching and exfoliation treatment.[65] The size of the obtained CDs ranged from 1 to 4 nm (Figure 1b) and could be controlled by changing reaction temperature. The top-down synthesis strategy achieves the transformation of 1D, 2D, and 3D carbon-based materials to 0D, which further expands the research scope of carbon. However, the high price of raw materials, complex preparation process, and relatively low yield rate lead to the high cost of CDs preparation.[66] Therefore, it requires researchers to find alternatives to expensive carbon sources and improve the synthesis methods of CDs.

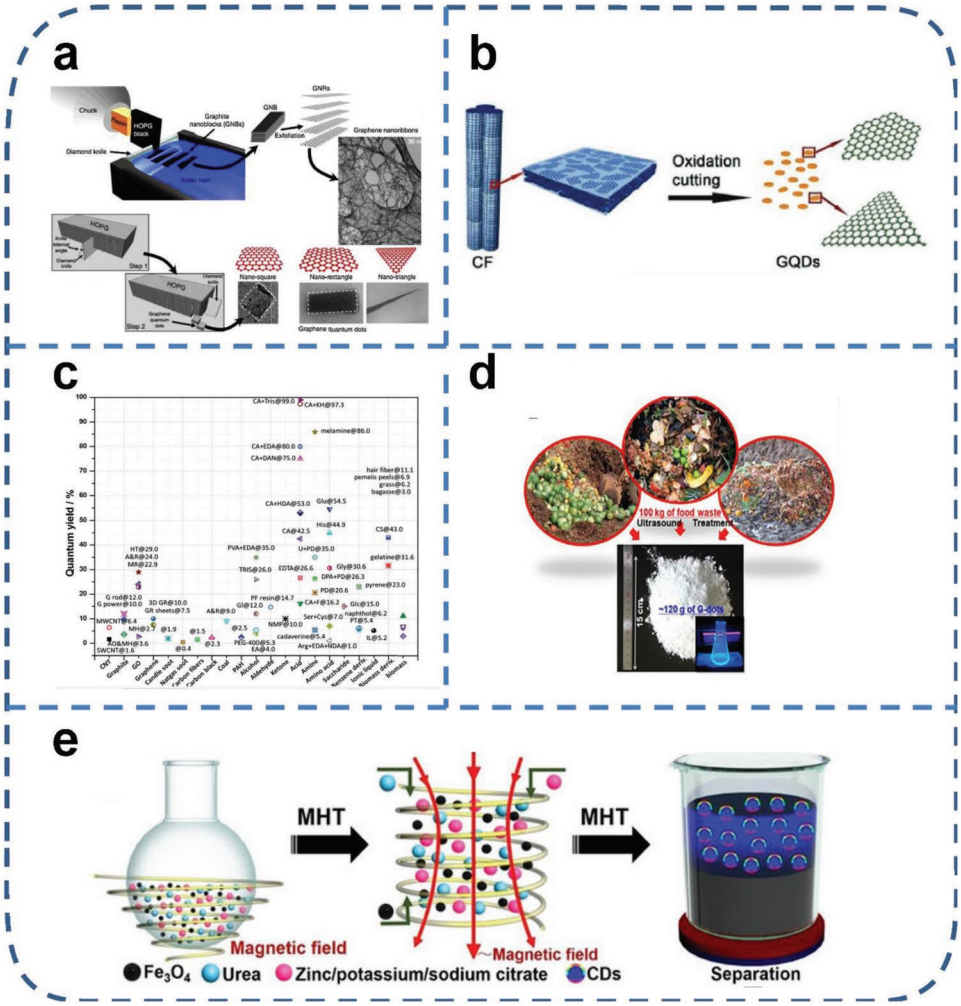

Figure 1. a) Schematic diagram of the graphite nano-blocks cutting and peeling process. Reproduced with permission.[64] Copyright 2012, Springer Nature. b) Schematic illustration of acid etching and exfoliating carbon fibers (CF) into CDs. Reproduced with permission.[65] Copyright 2012, American Chemical Society. c) QY of CDs prepared from different carbon precursors. Reproduced with permission.[67] Copyright 2019, Royal Society of Chemistry. d) Schematic diagram of the scale-up preparation of CDs by using food waste. Reproduced with permission.[68] Copyright 2014, American Chemical Society. e) Illustration of the large-scale production of CDs by MHT method. Reproduced with permission.[69] Copyright 2020, Wiley-VCH.

2.2.2. Bottom-up

The bottom-up preparation of CDs involves condensation, crosslinking, and/or carbonization of the small molecules via the hydrothermal method, pyrolysis treatment, and microwave-assisted synthesis. Compared to top-down strategies, bottom-up methods exhibited many prominent advantages such as lower cost, milder reaction conditions, and more available carbon sources. Besides, the CDs fabricated by bottom-up methods demonstrated well-defined morphology and high QY. The relation between QY of CDs from different carbon precursors was summarized by Sun's group (Figure 1c).[67] It was concluded that the CDs synthesized via bottom-up approaches usually have higher QY compared with top-town routes.

From both applied perspectives, easy large-scale preparation and turning waste into value-added materials maybe the most appealing characteristics of CDs synthesized via a bottom-up method. Park et al. proposed a facile and eco-friendly approach for the massive production of CDs with green fluorescence from food waste-derived sources. Through simple sonication of food wastes in a 10 vol% ethanol solution for 45 min, the CDs were obtained with a yield of up to 120 g per 100 kg of food waste (Figure 1d).[68] The prepared CDs can be used in biomedical imaging and water quality monitoring due to their high photostability and water solubility. Recently, a novel highly efficient magnetic hyperthermia approach to preparing multi-color fluorescence CDs was reported by Du and coworkers.[69] The efficiency of this method is 160 times higher than traditional hydrothermal methods. After 3 min reaction, more than 80 g CDs were obtained in one batch, with over 70% yield (Figure 1e).

At the end of the synthesis reaction of bottom-up methods, there are still unreacted molecules or ions in the solution. Before being used, raw CDs need to be purified. However, the purification of CDs is complex due to their small size, low density, and excellent water solubility. Therefore, they are hard to

isolate by common separation techniques, such as centrifugation and filtration.[70] Dialysis is the most frequently used technology during the CDs' purification process.[71] With this technique, macromolecular materials can be retained, and small molecules and ions unreacted can be diffused out of the bag until the concentration of the inside and outside of the bag is balanced. Gel chromatography is another attractive technology to purify CDs. By using low-pressure size-exclusion chromatography, Arcudi's group had successfully achieved the separation of CDs with different sizes and properties.[72] In addition, CDs powders are often used in many scenarios, such as characterization analysis, combination with other materials, etc. Freeze-drying and rotary evaporation are the most common technology to separate CDs from the liquid phase. Nonetheless, the aggregation of nanoparticles is still hard to avoid. The isolation and purification of CDs remain a significant challenge in the future.[73,74]

2.3. Modifications of Carbon Dots

2.3.1. Size and Shape Control

Due to quantum confinement effects, the size-dependent PL emission property is a prominent feature of CDs. Furthermore, the optical bandgap and electronic properties of CDs are also determined by size and shape. Chen and co-authors intensively studied the effects of size, edge configuration, and shape upon the bandgap and PL emission of CDs via theoretical calculation.[75] As shown in **Figure 2**a, the fluoresce emission was red-shifted with the increase of CDs size. They also revealed that CDs with different edge configurations showed apparent differences in the bandgap. In addition, the sizes of CDs often have a significant impact on the energy band structure, the degree of structural disorder, and the number of carrier recombination centers, which in turn affect their catalytic performance.[53,54] The effect of the size dependency of CDs on photocatalysis was discussed by Zhou et al.[76] They obtained CDs in three different sizes of ≈2, 3, and 5 nm using microwave-mediated method and exclusion chromatography. From the experimental results of Rhodamine B photodegradation by different particle size CDs, the catalytic activity of the as-prepared CDs was found to increase with decreasing particle size. The reason was that the size of the particle changed the bandgap of CDs as well as their ability to absorb light. In another research work on the photocatalytic conversion of CO_2, Nam and colleagues constructed a photocathode for reducing overpotential and improving CO selectivity by loading 3.6 nm N-CDs on p-type silicon nanowire (SiNW) arrays.[77] The density functional theory (DFT) calculation demonstrated that as the size increased from 0.96 to 3.40 nm, the bandgap of N-CD decreased significantly from 4.13 to 1.00 eV (Figure 2c), suggesting that N-CDs with larger size could efficiently harvest electrons from the conduction band of p-type silicon. Furthermore, the nanoconfinement effects of CDs maximize the exposure of pyridinic N atoms, which were the major active sites for enhancing the adsorption and binding abilities of CO_2.

However, it has been challenging to control CDs at specific sizes precisely. Researchers have made numerous attempts to obtain uniform and homogeneous CDs. Yuan et al. fabricated a series of multicolored narrow bandwidth emission triangular CDs by solvothermal treatment of phloroglucinol triangulogen (Figure 2b).[78] By regulating the dosage of H_2SO_4 and heating times, the sizes of CDs could be tailored from 1.9 to 3.9 nm and the QY could be as high as 54–72%. Moreover, these CDs derived multicolored luminous diodes showed excellent stability, high luminance, and outstanding color purity. In another report, Zhu's group proposed a strategy to synthesize CDs of controllable size by employing limited pyrolysis of organic precursors in nanoreactors.[79] Specifically, the carbon precursor was impregnated into the mesoporous silica spheres, and then the silica spheres' support was etched and washed to generate homogeneous CDs. The key of this method was to control the pore diameter of silica spheres, which influenced the size and size distribution of CDs. Recently, Atabaev et al. developed a facile synthesis method to tune the size of CDs by adjusting the reaction time and precursor concentration.[80] In the 0.075–0.125 g mL^{-1} precursor concentration range, the mean sizes of CDs are positively correlated with the concentration, and the mean diameter of CDs also increased with the reaction time.

Compared with size modulation, the shape regulation of CDs is more challenging. Kim et al. fabricated CDs with trilateral and quadrilateral morphology and multi-color (blue, green, and yellow) fluorescence emission, as shown in Figure 2d.[81] Phloroglucinol was selected as a carbon precursor and heated at 190 °C for 25, 50, and 90 min to obtain the blue, green, and yellow emitting CDs, respectively. The authors proposed the formation mechanism of CDs of different shapes that were regulated by dehydration polymerization and controlled growth in a sulfuric acid medium. However, due to the limited accuracy of existing synthesis methods, perfect CDs with precise cut shapes and single-crystalline structures are practically tricky to prepare. Until recently, Park's group proposed a new method based on a catalytic solution to synthesize the dimensionally-controllable hexagonal single-crystalline CDs (Figure 2e).[82] By controlling the reaction temperature, the sizes of these single-crystalline CDs could be tuned easily. This method is expected to develop into a general approach to preparing single-crystalline CDs.

2.3.2. Heteroatom Doping

Doping with heteroatoms is another widely applied strategy for the modification of CDs.[83] Heteroatoms can be introduced on the surface and the carbon core of CDs, which can produce more active sites and new energy levels and adjust the photoelectric properties of CDs.[46,84,85]

It was found that nitrogen (N) is the most common doped element in plenty of literature reports related to heteroatom doped CDs. This was attributed to the atomic radius similar to carbon and the strong affinity of lone pair electrons with the carbon sp^2 domain.[86] Zhu et al. prepared N-CDs with different nitrogen contents (9.8–17 wt%) via hydrothermal methods employing citric acid and ethylenediamine as the carbon and nitrogen source, respectively.[87] The QY of these N-CDs was up to 80% and could be produced on large scale with a yield of 58%. The optical performance of N-CDs was close to those

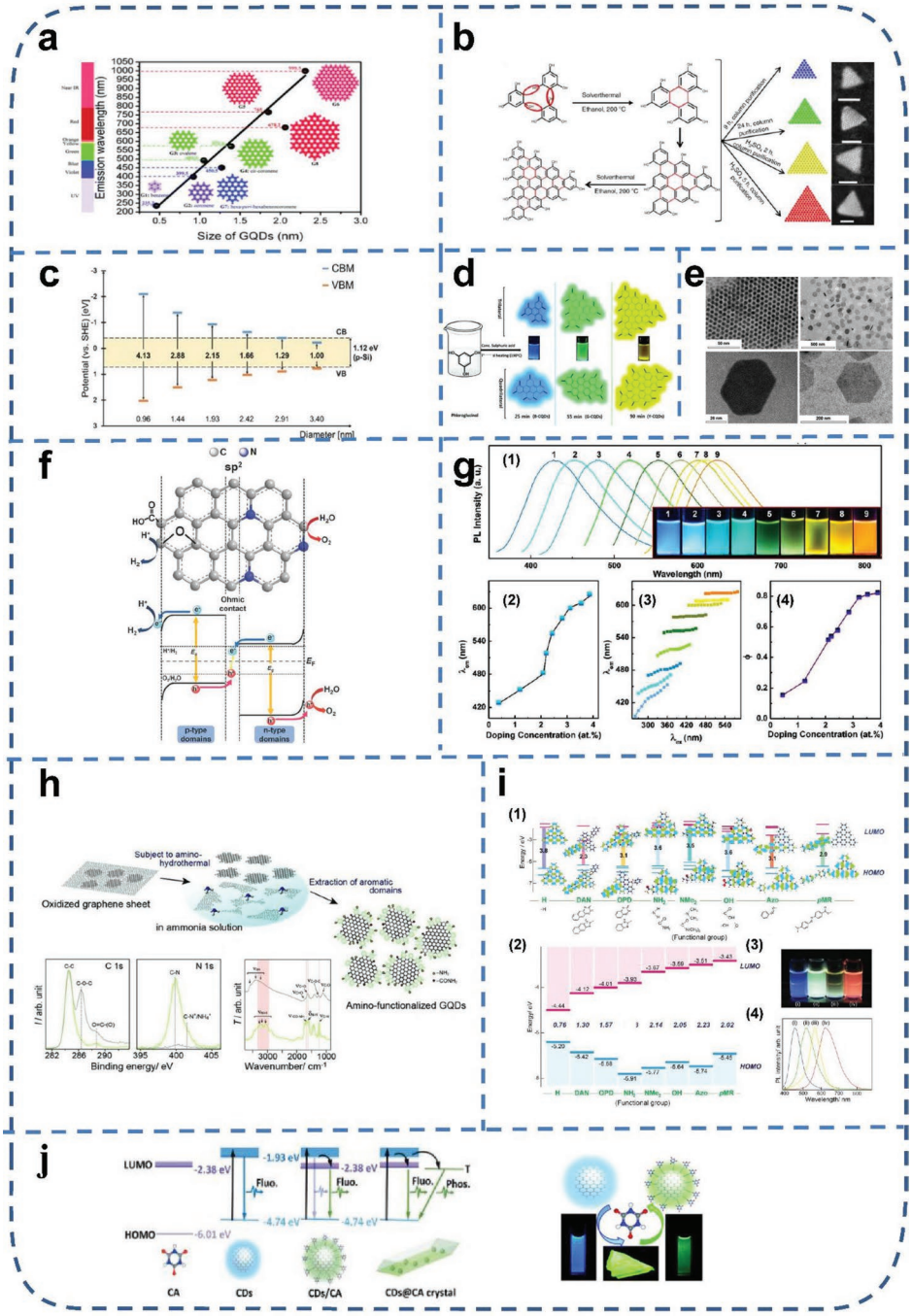

Figure 2. a) Schematic diagram of the relationship between the emission wavelength and the size of CDs calculated using the DFT. Reproduced with permission.[75] Copyright 2014, Royal Society of Chemistry. b) Synthesis schematic of multicolored emission triangular CDs by solvothermal treatment. Reproduced with permission.[78] Copyright 2018, Springer Nature. c) Band alignment of p-type Si and calculated band edge positions of different sized CDs. Reproduced with permission.[77] Copyright 2016, Wiley-VCH. d) Synthesis schematic of multicolor fluorescent (blue, green, and yellow) CDs with specific shapes (trilateral and quadrilateral). Reproduced with permission.[81] Copyright 2020, Royal Society of Chemistry. e) Transmission electron microscopic images of single-crystalline CDs with a hexagonal shape. Reproduced with permission.[82] Copyright 2019, American Chemical Society. f) Schematic diagram of photocatalytic water-splitting by N-CDs containing internal p-n interfacial junction. Reproduced with permission.[89] Copyright 2014, Wiley-VCH. g) Changes in the optical properties of S-CDs due to different doping concentrations: 1) PL spectra of S-CDs with different doping concentrations. 2) Relationship between doping concentration and excitation wavelength. 3) Relationship between emission wavelength and excitation wavelength. 4) QY of different S-CDs. Reproduced with permission.[95] Copyright 2018, American Chemical Society. h) Preparation process, XPS, and FTIR of amino-functionalized CDs. Reproduced with permission.[108] Copyright 2012, Wiley-VCH. i) Energy levels and photoluminescence for nitrogen-functionalized CDs: 1) Predicted energy level diagrams for CDs with various nitrogen-containing functional groups. 2) Measured energy level diagrams for N-CDs. 3) PL image of N-CDs in aqueous solution with UV lamp excitation. 4) Corresponding normalized PL spectra of the aqueous solution of N-CDs (excitation wavelength 380 nm). Reproduced with permission.[109] Copyright 2016, Wiley-VCH. j) Graphical representation of energy level and fluorescence variations of CDs, CDs/CA, and CDs@CA before and after the co-crystallization. Reproduced with permission.[110] Copyright 2020, Royal Society of Chemistry.

of commercial organic dyes and semiconductor quantum dots. Liu and co-workers used 4-nitrophenol as the precursor to fabricate N-CDs by solvothermal methods.[88] The as-prepared N-CDs exhibited strong NIR absorption (650–950 nm) and distinct up-convert PL emission properties. More interestingly, the N-CDs could convert the absorbed NIR into heat, and the photothermal conversion efficiency reached as high as 33.5%. In another report, Teng's group used the water-splitting reaction to demonstrate that nitrogen doping could change the semiconductor type of CDs.[89] The experiment showed that pristine nitrogen-free CDs deprived of graphene oxide (GO) could only produce H_2 under irradiation, proving p-type conductivity. While after the treatment of pre-calcining at 500 °C in NH_3, the NH_3-treated CDs exhibited the characteristics of n-type semiconductors and catalyzed only the production of O_2. Further oxidation of the NH_3-treated GO by modified Hummers' method, the obtained CDs resulted in the yielding of H_2 and O_2 at the molar ratio of 2:1 from water, which indicated that the p-n type photochemical diodes formed. It was reported that the surface oxygen species of CDs caused the p-type conductivity, and the n-type conductivity was generated by nitrogen atoms inserted in the CDs' frames, just as shown in Figure 2f.

Other non-metallic elements such as boron (B), fluorine (F), phosphorus (P), and sulfur (S) have also been successfully doped into CDs. B is a typical p-type doping element with fewer valence electrons but a similar dimension of atoms to carbon, so it can be easily doped into the CDs' lattice. Hai et al. proposed a facile one-pot microwave approach with GO and borax as reactants to prepare B-CDs.[90] The obtained B-CDs exhibited excitation-independent PL character and high QY (21%), which attributed to the incorporation of B atom into graphene structure to repair the defects in graphene lattice. Moreover, the excellent PL stability in the pH range of 3.0–11.0 and superior resistance to external high ionic concentration made it has great potential to detect contaminants in water. In another experiment, F-CDs with adjustable sizes and controllable fluorine contents were fabricated via a gradient fluorine-sacrificing strategy by Gong and colleagues.[91] Compared with nonfluorinated CDs, the as-synthesized F-CDs exhibited pH-independent fluorescence and stronger paramagnetism (5 times than pure CDs). Li and co-authors proposed that the doping of P atoms into CDs could lead to molecular aggregation due to the electron-rich properties of P, thus causing the increase in particle size and an extension of the electron system, which led to a red-shift of PL. They achieved the emission wavelength modulation of P-CDs in a wide range from 455 to 595 nm by adjusting the concentration of phosphoric acid in the hydrothermal process.[92] S is another common doping element, which can change the electron density and create more structural defects, resulting in more emissive traps and enhancing the QY of CDs.[93,94] In a report by Wang et al., they proposed a green and efficient strategy for the preparation of controllable lattice S-doped CDs via the hydrothermal processing of durian in the existence of platinum (Pt) catalysts.[95] The S atoms were doped into CDs' lattice during the efficient reforming cyclization of Pt, resulting in outstanding photoluminescent properties and ultrahigh QY (79%, higher than most CDs previously reported in the literature). They also demonstrated that the PL performance of CDs could be tuned by adjusting the S doping concentration during preparation, as shown in Figure 2g.

The co-doping strategies are also used to improve the synergistic effect among multiple heteroatoms and reform the electronic structure of doped CDs, further affecting their photochemical properties.[96] Zhao's group synthesized a novel tricolor F and N co-doped CDs (F,N-CDs) via the alkali-assisted method using wasted cucurbit flesh as C and F sources and urea as N source. By adjusting the NaOH concentration and changing the F and N contents, the obtained F,N-CDs exhibited green, yellow, and orange PL emissions, respectively. Besides, the tricolor F,N-CDs possessed outstanding photocatalytic degradation activity of organic dyes. More importantly, the degradation rate gradually increased with the PL redshift of F,N-CDs. In another report, S and Cl doped CDs from waste palm powders and thionyl chloride were fabricated and showed excellent photocatalytic performance for the degradation of organic contaminants under visible light.[97] With the S and Cl incorporation, the photogenerated electrons and holes were trapped at several surface defect sites of the doped CDs and then reacted with adsorbed oxidizing/reducing substance on the surface, thus generating conducive active radicals to photodegradation.

Similar to the doping of non-metal elements, some metal elements are also beneficial to improving CDs' performance. Khare and co-workers fabricated soluble zinc-doped CDs (Zn-CDs) with high QY (72%) and brightly red fluorescent via microwave methods using bougainvillea plant leave as C source and zinc acetate as Zn source.[98] The photostability of Zn-CDs was close to that of commercial quantum dots and organic dyes. Recently, cobalt-doped CDs (Co-CDs) were prepared through the hydrothermal treatment of 1-(2-Pyridylazo)-2-naphthol and cobalt chloride.[99] The Co-CDs showed two emission peaks generated by the fluorescence resonance energy transfer (FRET) from different nanoparticles. Specifically, since the short-wavelength emission band of CDs is overlapped with the cobalt-related absorption zone, the short emission light can be reabsorbed during the process of cobalt-related leap followed by emission as cobalt-related radiation in the long-wavelength range.

2.3.3. Surface Modification

It has been proved that the photoelectric performance of CDs is heavily affected by their PL properties, bandgaps, charge transfer rate, and separation efficiency of hole-electron pairs, which relate to the electronic structure in their carbon cores, fluorophores, or surface chemical groups.[100–107] Surface modification of CDs has been considered to be an effective way to tune their photoelectric characteristics.

To tune the PL properties of CDs, Tetsuka's group fabricated a novel amino-functionalized graphene nanostructure via ammonia-mediated cutting of oxidized graphene sheets.[108] The oxidized graphene sheets were subjected to moderate hydrothermal processing in an ammonia solution at no more than 150 °h to avoid damaging the graphene structure. Through the soft bond-scission process, the epoxide ring at the edge of graphene was opened and simultaneously directed bonded with a primary amine. Thus, size-controlled CDs of edge-termination structure with primary amine were obtained (Figure 2h). Furthermore, it was found that the PL of the amino-functionalization CDs can be tailored from violet to the visible region

under 365 nm irradiation by adjusting the degree of terminal amination. Based on the above research, Tetsuka et al. further proposed a nitrogenous functionalization strategy for designing and tuning the energy levels and bandgaps of CDs.[109] They combined nitrogen-containing precursors with oxidized CDs in nucleophilic substitution and dehydration reactions to obtain a series of nitrogen-functionalized CDs. Experimental measurements and theoretical calculations proved that the HOMO and LUMO levels of N-CDs achieved continuous modulation (Figure 2i). In another report, Zhou et al. functionalized CDs with cyanuric acid (CA) via a simple co-crystallization process to change the original blue fluorescence to green.[110] The mechanism behind this phenomenon is that the CA molecules firmly bonded with CDs through hydrogen bonds. The photoexcited electrons of CDs@CA shifted from high energy LUMO levels of CDs to LUMO levels of surface-bonded CA molecules and then recombined to the HOMO levels of CDs via emitting green light, just as shown in Figure 2j. Moreover, some researchers designed and fabricated N or Cl decorated CDs to evaluate the influences of different surface heteroatoms upon their PL and photocatalytic performance.[111] They prepared the pristine CDs by hydrothermal method using ethylene glycol as the carbon source. Then adding ammonia solution or thionyl chloride molecules into the above-obtained suspension for 5 h reaction, to form N- or Cl-contained radicals on the CDs' surface. The existence of nitrogenous groups in CDs resulted in stronger PL activity, while chlorine-containing groups led to enhanced photocatalytic performance. The reason behind the discrepancy may be due to the difference in the directions and degrees of N- or Cl- radical-induced energy band bending from the interior to the surface.

During the synthesis of CDs, oxygen-containing groups are typically produced on the surface. Nevertheless, the difference in the extent of oxidation on CDs' surfaces can cause the alteration of radiative recombination of localized e^-/h^+ pairs and change the number of emissive traps, thus affecting structure defects and optical properties.[112–114] Zhu and colleagues fabricated oxidized-CDs (o-CDs) and reduced-CDs (r-CDs) via post-treatment of hydrothermal synthesized CDs by oxidation and reduction strategies.[115] It was found that the as-prepared CDs exhibited blue (pristine CDs), green (o-CDs), and red-emissions (r-CDs), respectively. They systematically analyzed the morphology, emission spectra, UV–vis absorption spectra, and Fourier transform infrared reflection (FTIR) spectra of the above CDs. The results revealed that the different color light emissions were associated with the three surface states: the intrinsic, C=O− and C=N−, respectively. In another report, three types of CDs with similar sizes and heights but different degrees of surface oxidation via the solvothermal method were obtained.[116] With the increasing degree of surface oxidation, the emission spectra of these CDs exhibited red-shifted emission and the QY achieved 4.1%, 9.9%, and 12.2%, respectively. The variation of optical properties of CDs was mainly attributed to the more surface defects induced by a higher degree of surface oxidation. To further illustrate the relationships between the different surface oxidation states of CDs and fluorescence, the authors treated green CDs (5.9% of QY) with $NaBH_4$ and the fluorescence of CDs turned blue and the QY increased to 12.1%.[117] They revealed that these oxygen-containing groups (carboxyl, epoxy, and amido moieties) on the CDs' surface were partially converted to −OH groups during the process of reduction, thus the non-radiative process was suppressed.

Surface passivation is another method of surface modification, which is to construct a thin surface protective layer by grafting organic polymers on the terminal of CDs, thus prolonging their fluorescent lifetime and reducing photo corrosion.[118] The surface-passivated CDs exhibited better PL properties than "naked" CDs. The surface passivation treatment eliminated the dissipation of photoexcited carriers from surface sites and led to more highly efficient radiative recombination.[119,120] So far, the most popular surface passivator includes organic molecules and polymers, such as polyethylene glycol (PEG), polyethyleneimine (PEI), and poly(propionylethyleneimine-*co*-ethyleneimine), which are non-emissive in the UV–vis spectrum. Xue and colleagues proposed a facile PEI-assisted hydrothermal cutting method to fabricate nearly monodisperse CDs with uniform size.[121] In this research, branched PEI, as a chemical scissor and stabilizer, cut oxidized graphene sheets into little peace and prohibited CDs from layer stacking and later aggregation in the preparation process. The modified CDs showed sharper band-edge absorption, narrower PL peak, and higher QY (21%). Moreover, Teng et al. found that CDs' PL could be tuned by surface passivation with PEG of different molecular weights (Mw), and these passivated CDs showed a linear correlation between PL intensity and Mw of PEG.[122] Besides, Wu and co-workers synthesized CDs derived from food-grade honey and the PL properties of these CDs were significantly enhanced by utilizing hyperbranched polymers as surface passivator.[123] In contrast with CDs treated with linear PEG-400, the average radiant efficiency at the NIR range for hyperbranched polymer passivated CDs increased dramatically, due to the increased surface area available for light passivation.

3. Carbon Dots-Based Sensors for Air Pollutants Detection

Since the superior characteristics such as low biotoxicity, tunable fluorescence, rich surface functional groups, and excellent electrical conductivity, CDs have been increasingly employed as sensing materials for gaseous pollutants detection in recent years. According to recent reports, CDs-based sensors for gas pollutant detection can be classified as conductometric sensors and optical sensors (as summarized in **Table 1**). The specific mechanisms and applications will be described below.

3.1. Optical Sensors

CDs with multiple functional groups can easily interact with gas molecules that have different electronic structures in the surrounding environment, leading to the change of inherent fluorescence properties, such as fluorescence quenching or emission peaks shift or fluorescence enhancement or FRET.[124] The distinctive optical signals generated by the interaction of gas molecules with CDs can be used to detect gas contaminants. Moreover, CDs can be directly dissolved in solvents

Table 1. CDs-based sensors for air pollutants detection.

A. Optical sensors

Serial number	Sensing materials	Target air pollutants	Sensing mechanism	Range of detection	Limit of detection	Ref.
1	BPEI-CDs/silica aerogels	NO_2	Fluorescence quenching	2–10 ppm	250 ppb	[171]
2	CDs/PVDF film	NH_3	Fluorescence quenching	1.7–10 000 ppm	1.7 ppm	[128]
3	CDs/cotton substrate	NH_3	FRET	0–200 ppm	3 ppm	[133]
4	CDs solution	Acetone	Fluorescence quenching	8.75×10^{-7} M		[125]
5	Mn-CDs/PVDF film	Cyclohexane, toluene, 1,4-dioxane, chloroform, methylene chloride, acetone, acetonitrile, ethanol, methanol, glycol, and water	FRET			[172]
6	Amphiphilic CDs	Dichloromethane, ethylacetate, tetrahydrofuran, dimethylformamide, acetonitrile, methanol, ethanol, acetone, and water	Difference of fluorescence color			[173]
7	CDs-aerogel	Benzene, aniline, o-, m- and p-phenylenediamine, nitrobenzene, phenol	Fluorescence quenching	0–150 ppm	Below 5 ppm	[174]
8	N-CDs solution	NO_x	Fluorescence quenching	3.77–36.51 ppt and 27.67–43.77 ppt	1.41 ppt	[127]
9	S-CDs solution	NH_3	Fluorescence quenching	0–800 ppm		[175]
10	S,N-CDs solution	Acetone	Fluorescence quenching	0–0.05 M	7.2×10^{-7} M	[126]
11	Ag-CDs solution	H_2S	FRET	$1–1900 \times 10^{-9}$ M	0.4×10^{-9} M	[176]
12	N,B-CDs solution and N,B-CDs/PVA film	Acetone	Fluorescence enhancement	$0–800 \times 10^{-6}$ M	0.54×10^{-6} M	[134]
13	MCM-41/CDs	Acetic acid	Fluorescence enhancement	0–9.5 µmol L^{-1}	0.2 µmol L^{-1}	[177]
14	CDs/CNF aerogel	NO_x and aldehyde	Fluorescence quenching	1–100 ppm (aldehyde)	-	[129]
15	CDs–PNBD solution	H_2S	Ratiometric fluorescence change	$0–35 \times 10^{-6}$ M	57×10^{-9} M	[138]
16	CDs solution	H_2S	Ratiometric fluorescence change	$0–800 \times 10^{-6}$ M	7×10^{-9} M	[142]
17	CDs film coated on glass slide	Methanol, ethanol, dichloromethane, tetrahydrofuran, and hexane	Difference in optical absorbance			[55]
18	N-CDs/optical fiber	Methanol, ethanol, and propanol	Difference in transmitted light intensity	50–300 ppm	4.3 ppm (methanol) 4.9 ppm (ethanol) 10.5 ppm (propanol)	[178]
19	CDs film coated on glass slide	NH_3	Difference in optical absorbance and fluorescence enhancement	0–30% (volume fraction of NH_3 in water)		[179]
20	CDs film coated on glass slide	Acetone	Difference in optical absorbance and fluorescence enhancement	1–100% (volume fraction of acetone in water)		[143]
21	TiO_2/AF-CDs film	H_2S	Interferometric wavelength drift	0–55 ppm		[145]

B. Conductometric sensors

Serial number	Sensing materials	Target air pollutants	Sensing mechanism	Sensing range	Limit of detection	Response/ recovery time	Temperature	Ref.
22	N-CDs/PEDOT-PSS	Methanol, ethanol, acetone, toluene, chlorobenzene, propanol	Resistance change	1–1000 ppm	5 ppm	12 s/32 s	Room temperature	[180]
23	Acidic and neutral CDs coated ITO	NH_3	Current change	10–400 ppm		26 s/21 s (acidic CDs) 27 s/72 s (neutral CDs)	Room temperature	[149]
24	S,N-CDs/PANI	NH_3	Resistance change	1–1000 ppm	0.5 ppm	115 s/44 s	Room temperature	[168]

Table 1. Continued.

Serial number	Sensing materials	Target air pollutants	Sensing mechanism	Sensing range	Limit of detection	Response/ recovery time	Temperature	Ref.
25	rGO/CDs	NO_2	Current change	0.05–25 ppm	0.01 ppm	100 s/150 s	Room temperature	[151]
26	CDs/SiNW array	NO_2	Current change	10–500 ppm	10 ppm		Room temperature	[170]
27	PtO_x/CDs/TiO_2 film	Isopropanol	Resistance change	0.1–40 ppm		9 s/-	Room temperature	[181]
28	CDs-TiO_2	Isopropanol	Resistance change	2–500 ppm		18 s/11 s	Room temperature	[166]
29	B-CDs/Ag-$LaFeO_3$	Formaldehyde	Resistance change	1–30 ppm		20 s/30 s	55 °C	[169]
30	CDs/In_2O_3	NO_2	Resistance change	50–500 ppb	9 ppb	9.6 min/5.3 min	50 °C	[164]
31	CDs/SWCNTs	NO_2	Resistance change	3.3–42 ppm	18 ppb	381 s/294 s	Room temperature	[153]
32	N-CDs/In_2O_3	NO_2	Resistance change	0.1–3 ppm	100 ppb	95 s/36 s	100 °C	[163]
33	CDs/SnO_2/ZnO	H_2S	Resistance change	0.025–5 ppm	0.1 ppm	14 s/13 s	Room temperature	[165]
34	N-CDs/TiO_2 graphene foam	Formaldehyde	Resistance change	6.1–40 ppb		16 s/18 s	150 °C	[152]
35	CDs-coated microchannel	Toluene, hexanal, hexane, pentanol, propanol, ethanol, and methanol	Resistance change					[150]
36	N-CDs/SnO_2	NO_2	Resistance change	0.2–1 ppm	0.1 ppm	59 s/33 s	130 °C	[158]
37	N-CDs/ZnO	NO_2	Resistance change	0.1–100 ppm	44.5 ppb		100 °C	[182]

containing contaminant composition for fluorescence detection or combined with some porous materials or polymer matrix to fabricate solid-based sensors.[25]

3.1.1. Fluorescence Quenching Response

Jayasmita et al. synthesized CDs with strong blue fluorescence via modified hydrothermal methods.[125] They further observed the fluorescence phenomenon of the prepared CDs dissolved in different water-miscible solvents. It was found that the fluorescence of CDs dissolved in aqueous acetone solution was quenched and the reduced fluorescence intensity was linearly related to acetone concentration. The fluorescence quenching was mainly attributed to acetone as an excellent electron donor to stabilize the holes on the surface of CDs, thus hindering radiative recombination, as shown in **Figure 3**a. Similarly, Narayan's group fabricated S,N-CDs as fluorescent nanoprobe to selectively detect acetone in human fluids.[126] The incorporation of S and N significantly improved the luminescence property of CDs and provided identification sites for achieving specific detection of acetone. Based on the principle of fluorescence quenching, the N-CDs prepared by Mohammad and his colleagues were applicable for the detection of NO_x at ppt levels.[127] Specifically, a certain amount of NO_x gas was loaded into 2 mL aqueous solutions of CDs by nitrogen gas, and the time of purging NO_x was controlled by an electronic valve linked to a computer. Subsequently, the fluorescence intensity of the CDs solution was measured.

Solid sensors have more advantages than liquid-based sensors, such as the superior ability to adapt to more complex scenarios, more accessibility to operate, and better portability. Hence, it is a promising strategy that CDs to be embedded on films or porous materials to build composite fluorescent sensors, which have dual functionality for analytes enrichment and intuitive optical recognition. Liang and his co-workers developed a simple, low-cost strategy to synthesize red fluorescent CDs via carbonization treatment of bagasse and further coated the prepared CDs onto polyvinylidene fluoride (PVDF) membrane to fabricate a solid-state fluorescent sensor for toxic gas monitoring.[128] The CDs/PVDF film could selectively distinguish NH_3 from other toxic gaseous analytes through sensitive fluorescence quenching (Figure 3b). And the curve of fluorescence quenching efficiency versus ammonia concentration was following the Langmuir equation, indicating that the quenching efficiency was in proportion to the adsorption amount of NH_3. Moreover, the authors first revealed the mechanism of chemical state transformation on the surface of CDs in solid-state. It was found that the fluorescence irreversible quenching of CDs exposed to the ammonia atmosphere was due to the NH_3-induced Michael addition reaction, which altered the graphite-like structure of the CDs by inserting N into the C = C group. Whereas, the deprotonation of the −COOH by the formation of the $-NH_4^+$ resulted in reversible fluorescence quenching. This assumption was proved by a reversible sensing test, where fluorescence could be partially restored after air purging for 150 s.

Lin et al. proposed a novel strategy to fabricate composite fluorescent aerogels by linking cellulose nanofibril (CNF) and fluorescent CDs through covalent bonding.[129] The compression strength of the CDs/CNF aerogels improved by 360%, and the capability of shape recovery in water significantly developed due to being covalently bonded with CDs nanoparticles. More importantly, the aerogel exhibited high selectivity and sensitivity for sensing NO_x in gas and aldehyde species in water. In contrast to the slight fluorescence variation in N_2, CO_2, and SO_2 atmospheres, the CDs/CNF aerogel exhibited fast and complete fluorescence quenching in NO_x-containing environments. Regarding the aqueous aldehyde species detection, the CDs/CNF aerogel showed higher selectivity to the formaldehyde and glutaraldehyde among different types of organic aqueous

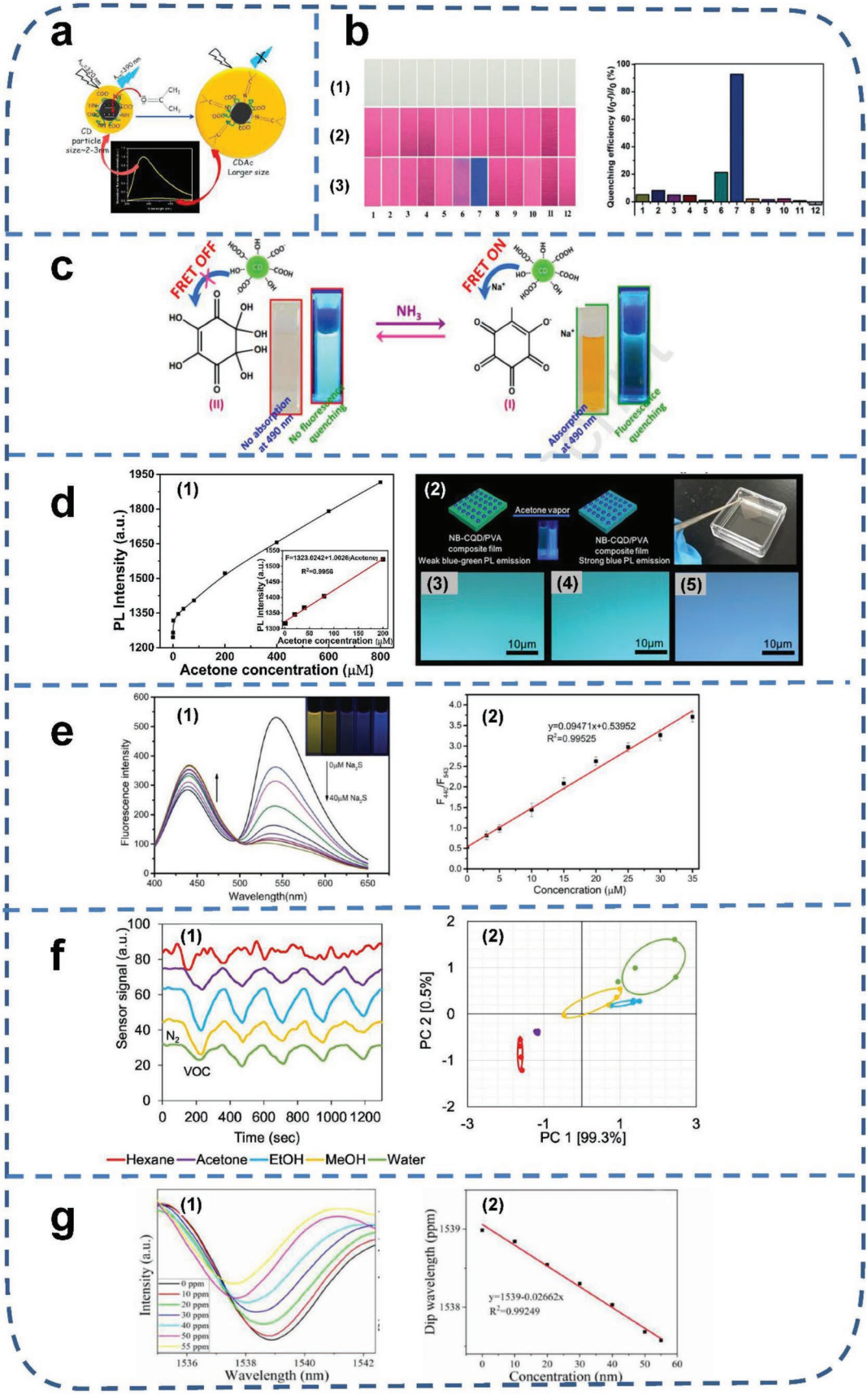

solutions. Moreover, the degree of fluorescence decay of aerogels was proportional to the glutaraldehyde concentration in the range of 1–100 ppm, indicating the great potential of this aerogel for both water and air quality monitoring. The fluorescence quenching mechanism of CDs toward NO_x and aldehyde species may attribute to the restricted radiation recombination of the electrons from the interaction between electron donors (CDs) and absorber (NO_x) and the covalent reactions between aldehyde groups and surface amino groups of CDs.

3.1.2. Fuorescence Resonance Energy Transfer Response

If the emitting spectrum of a donor is overlapping with the absorption spectrum of another recipient, meanwhile the length between the two fluorescent groups is suitable (<10 nm), the phenomena of FRET can be observed.[130] In recent years, this FRET-based fluorescence sensing strategy has been explored and attracted increasing attention in gas contaminant detection.[130–132] Manjunatha et al. successfully fabricated a sensing platform based on the FRET principle for ammonia detection in solution and gas phases by using CDs as donors and sodium rhodizonate as acceptors.[133] Pure sodium rhodizonate showed visible light absorption at 445 and 485 nm. Once the CDs solution was added, the sodium rhodizonate's characteristic absorption bands disappeared but exhibited blue fluorescence of CDs under UV light irradiation. This phenomenon was due to the presence of a large number of −COOH groups on the surface of CDs, which led to the protonation of rhodizonate (I) and the formation of rhodizonate (II) structure with a 356 nm absorption band. When aqueous ammonia was introduced into the sensing solution comprised of rhodizonate (II) and CDs, the fluorescence in the blue region (emission band centered at 490 nm) of CDs was quenched subsequently. The reduced intensity of fluorescence was positively correlated with the concentration of ammonia. Besides, the absorption bands at 445 and 485 nm were reappeared and enhanced with increasing ammonia concentrations, confirming that rhodizonate (I) was formed from the deprotonation of rhodizonate (II). According to the overlap of the blue region emission spectrum of the CDs and the absorption band of sodium rhodizonate, the existence of FRET between the donor (CDs) and acceptor (sodium rhodizonate) could be speculated, which led to the quenching of the CDs' emission after the introduction of ammonia. The mechanism of ammonia detection based on FRET was shown in Figure 3c. Furthermore, the cotton fibers coated with the sensor solution achieved selective identification of ammonia vapors at low concentrations (3 ppm), with good reversibility, high selectivity, and stability.

3.1.3. Fluorescence Enhancement Response

In addition to the fluorescence diminished response, there is another strategy to detect gaseous pollutants by improving the fluorescence intensity of sensing materials. Many mechanisms for such fluorescence enhancements are revealed, such as changing the surrounding environment, electron migration paths, and hindrance of nonradiative decay.[124] Fluorescence enhancement of N,B-CDs in the detection of acetone vapors was observed in Liu's report.[134] The functional N,B-CDs synthesized via the hydrothermal carbonization method showed solvent polarity-dependent PL properties. Figure 3d showed that the PL emission intensity at 490 nm increased linearly with acetone concentration within the range of 1–200 μM. The N and B decorated CDs/polyvinyl alcohol (N,B-CDs/PVA) composite film was further prepared and could be used for the visual detection of acetone vapor under an excitation light of 365 nm. When the composite film was exposed to an air atmosphere containing acetone, its color changed from blue-green to blue under UV light. Two explanations were elucidated for the increase of PL intensity: 1) The acetone molecules coordinate with the N,B-CDs, leading to surface passivation.[135] 2) The strong electron-withdrawing ability of B.[136] Acetic acid (HAc) was a typical acidic organic volatile compound associated with gaseous pollutant release, fuel combustion, and food spoilage. Xia and co-workers fabricated a fluorescent composite comprising ordered mesoporous materials MCM-41 and CDs to detect HAc solution and gas. The hybrid material was more sensitive to HAc gas than HAc solution due to the outstanding gas enrichment capability of MCM-41. Hence, combining CDs with novel porous materials to enhance fluorescence response by enriching analyte concentration is a promising gas sensing strategy.

3.1.4. Ratiometric Fluorescence Response

Ratiometric fluorescence is a unique analytical approach to identifying the target by measuring the ratio of fluorescence intensity at two different characteristic wavelengths as a signal parameter. Since the measured fluorescence ratio signal is

Figure 3. a) Mechanism diagram of fluorescence quenching of CDs induced by acetone. Reproduced with permission.[125] Copyright 2016, Elsevier. b) The CDs/PVDF solid-based fluorescence sensor for toxic gas detection: Photographs (left) of the CDs/PVDF films under 1) visible light, 2) before, and 3) after exposure to different toxic vapors under UV irradiation. Histograms (right) of different fluorescence quenching efficiencies of the composite films to the above analytes. Reproduced with permission.[128] Copyright 2015, MDPI. c) Schematic diagram of ammonia sensing based on FRET principle. Reproduced with permission.[133] Copyright 2016, Elsevier. d) Fluorescence enhancement of N, B-CDs in acetone vapor detection: 1) Plot of PL emission intensity versus acetone concentration. 2) Schematic diagram of N, B-CDs/PVA composite film for acetone vapor detection. 3–5) PL microscopy photographs of N, B-CDs/PVA composite film under UV light irradiation: Under initial conditions, exposure to room air, and treated with acetone vapor, respectively. Reproduced with permission.[134] Copyright 2019, Elsevier. e) The CDs-based ratiometric fluorescence probe for H_2S detection: 1) Fluorescence spectra of CDs/P-NBD in the presence of different concentrations of H_2S (0–40 mM). 2) Ratiometric fitting curve of F440/F543 with H_2S concentration. Reproduced with permission.[138] Copyright 2020, Royal Society of Chemistry. f) The identification of acetone by CDs-integrated electronic nose: 1) Sensing signals of CDs film in various gases under UV irradiation. 2) PCA score plots for different vapors. Reproduced with permission.[143] Copyright 2019, Elsevier. g) The detection of H_2S by TiO_2/AF-CDs deposited fiber optic sensor: 1) The spectral responses of the sensor in various concentrations of H_2S. 2) Linear fitting of the wavelength drift upon the concentration of H_2S. Reproduced with permission.[145] Copyright 2020, IOP Publishing Ltd.

independent of light source intensity and instrument sensitivity, the ratio fluorescence probe has high sensitivity, excellent selectivity, and wide linear range. Wang et al. reported a ratiometric fluorescence probe combined nitro-benz-2-oxa-1,3-diazole (NBD)-based derivative P-NBD with CDs to selectively detect H_2S.[137,138] The fluorescent nanohybrid showed two fluorescence bands with centers of 440 and 543 nm, belonging to P-NBD and CDs, respectively. Once exposed to H_2S, the fluorescence of CDs/P-NBD at 543 nm was quenched, whereas the intensity of the emission band at 440 nm was enhanced under a 365 nm UV light (Figure 3e). Moreover, the fluorescence intensity ratio (F_{440}/F_{543}) of the probe gradually linearly increased with the H_2S concentration in the range of 0–35 mM, and the limit of detection could reach 57 nM, much lower than other methods reported in the literature.[139–141] Recently, Yu et al. observed compelling luminescence phenomena of CDs passivated with PEG, which could be used as a dual ratiometric fluorescent probe to detect H_2S.[142] After the addition of Na_2S to the passivated CDs solution, the plots of the emission intensity ratios of F_{450}/F_{350} and F_{455}/F_{523} against the concentration of Na_2S exhibited an excellent linear relationship from 0 to 800 μM. Moreover, the detection limit was low to 7.0 nM, indicating this CD-based probe was the most sensitive for H_2S sensing reported so far.

3.1.5. Other Optical Response

Several optical sensing methods using fluorescence changes of CDs-based materials as analyte identification signals have been described above. Apart from that, there are some researches for gas detection using the difference in light absorption and light refraction of CDs-based sensors in different atmospheres. The electronic nose is a sensory system that mimics the animals' smell, including a light source, sensing materials, and light detector. When the sensing materials are exposed to vapors, the electronic nose can detect optical absorbance changes. Owing to the superior light-sensitive property, CDs can be used as a sensing layer in the electronic nose. Peerasak et al. fabricated a CDs-integrated electronic nose and achieved the recognition of acetone from hexane, ethanol, methanol, and water vapors by using the principal component analysis (PCA).[143] The sensor signals reflected the variation in light transmission in the different gases as shown in Figure 3f. In addition, the PCA scope plots showed that acetone had the minor zone, suggesting the acetone detection signal was the most reproducible. They further demonstrated that the change of electronic states caused by the interfacial interaction between VOCs and quantum dots induced the variation in the optical absorption of CDs through theoretical calculations.

The fiber optic sensor is a novel type of sensor that measures the interferometric wavelength drift caused by adsorption with the target gas.[144] It has been attracting more and more attention because it can be applied to long-distance without electricity, low temperature, flammable and explosive scenarios. In a recent report by Huang et al., they deposited titanium dioxide compounded with amino-functionalized carbon dots (TiO_2/AF-CDs) on the surface of photonic crystal fiber (PCF) as a sensing layer to detect H_2S.[145] As shown in Figure 3g, the output spectrum of the fabricated TiO_2/AF-CDs/PCF sensor showed a remarkable blue shift with the increase of H_2S concentration, and the fitted curve of central wavelength versus concentration of H_2S showed excellent linearity with a correlation coefficient of 0.99249 from 0 to 55 ppm. Additionally, the interference wave troughs of composite fiber sensors did not change in the temperature scope of 0 to 60 °C, indicating the sensors had the potential for practical application.

3.2. Conductometric Sensors

Conductometric sensors are generally based on the electrodes' changes in resistance or current due to the mutual electronic interaction of the analysis substrates and the analyte.[146] Compared to traditional gas detection methods, the electrical approach has the advantages of rapid measurement, low cost, and high selectivity.[147] At present, many nanomaterials including conducting polymers, metal oxides, and novel carbon nanocomposites have been reported to be designed as sensing substrates for conductivity sensors.[148] CDs have outstanding application potential among various functional materials owing to their simple preparation, super-large specific surface area, unique electronic properties, and significant functional groups. The following section will focus on the applications of CDs-based conductivity sensors for gas pollutants detection.

3.2.1. Pure Carbon Dots as Sensing Substrates

The types of functional groups on the CDs' surface can be modulated by choosing different precursors and controlling the synthesis conditions, thus altering their properties of conductivity and adsorption. These controllable characteristics facilitate the regulation of the CDs-based conductor sensors' performance. Guo's group fabricated two types of ammonia gas sensors based on CDs with different functional groups.[149] The CDs were prepared under different pH conditions, one was acidic and the other was neutral. When exposed to the ammonia atmosphere, both sensors showed good selectivity responses but with contrary resistance behavior (**Figure 4**a). As for the comparison of quantitative relationships, with increasing ammonia concentration in the scope of 0–400 ppm, the response value of acidic CDs sensors increased exponentially, while neutral CDs varied linearly. Besides, the sensors made of neutral CDs exhibited stronger resistance to water interference. Since acidic CDs sensors have a large amount of hydroxyl and carboxyl groups on their surface, when the functional groups are exposed to NH_3 gas and a certain amount of water vapor, they tend to ionize and react with NH_3 to form NH_4^+. Therefore, a large number of unprotonated carboxyl groups led to lower resistance of the sensor. Nonetheless, the increase in resistance of neutral CDs sensor was caused by the depletion of holes due to the transfer of electrons from NH_3 to CDs. Additionally, the surface of the neutral CDs sensor was hydrophobic, so its response to ammonia does not change under different humidity conditions. In another report, Mina et al. improved the selectivity by 101.45% and 98.82% of the microfluidic gas sensors toward polar and nonpolar VOCs by introducing the CDs to the

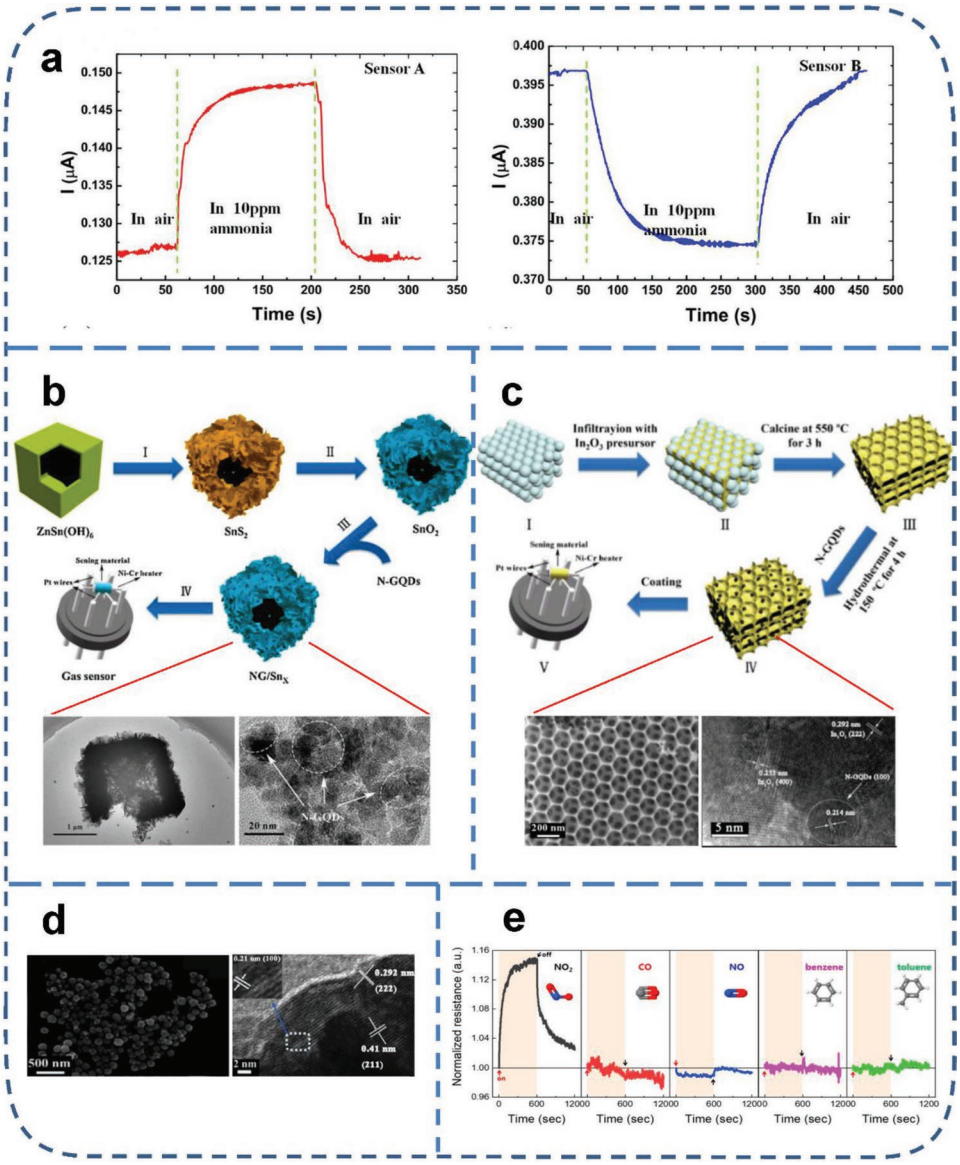

Figure 4. a) The ammonia gas response on CDs-sensors with different functional groups: ammonia response behavior of acidic CDs sensor (left), and ammonia response characteristic of neutral CDs sensor (right). Reproduced with permission.[149] Copyright 2016, Elsevier. b) Preparation schematic diagram and SEM/TEM images of N-CDs modified SnO_2 hierarchical hollow cube sensor. Reproduced with permission.[158] Copyright 2021, Elsevier. c) Synthesis illustration and SEM/TEM images of N-CDs modified 3DOM In_2O_3. Reproduced with permission.[163] Copyright 2020, American Chemical Society. d) SEM and TEM images of hierarchical In_2O_3/CDs nanospheres. Reproduced with permission.[164] Copyright 2020, Elsevier. e) Selectivity of the CDs-decorated SWCNT gas sensor. Reproduced with permission.[153] Copyright 2020, MDPI.

microchannel walls.[150] The introduction of CDs had a dual effect on improving VOC absorption: increasing the specific surface area of the microfluidic channels and grafting hydroxyl and carboxyl groups.

3.2.2. Carbon Dots/Carbon Nanomaterials as Sensing Substrates

Carbon nanomaterials, including reduced graphene oxide (rGO), fullerene, carbon nanotubes (CNTs), as well as carbon fibers, have unique features, such as high specific areas, large pore volumes, excellent chemical stability, and superior electrical conductivity. Significantly, their impedance can be changed when various gas molecules are attached or detached from their surface. Among these carbon nanomaterials, rGO with 2D structure and residual oxygenated groups could facilitate electron transport and chemical modifications, which was recommended as an ideal material for gas sensors. Su et al. designed an all-carbon nanoscale heterojunction sensing material consisting of rGO and CDs.[151] The CDs were in situ anchored on the rGO surface via a simple hydrothermal treatment. The addition of CDs boosted the NO_2 sensing performance by 3.3 times compared to the pristine rGO-based sensor and CDs/rGO nanocomposite had an ultra-low NO_2 detection

limit (10 ppb). Moreover, after six consecutive cycle tests and unencapsulated -storage for 90 days, the samples still showed high sensing performance. It was found that the CDs increased the hole density of the rGO's surface and enhanced the interfacial charge transfer between heterojunctions.

The 3D framework graphene can offer a seamless network with high conductivity and large specific surface area, which is suitable for loading 0D nanomaterials to achieve synergistic effects. Recently, Shao et al. deposited Au decorated N-CDs/TiO_2 microspheres uniformly on graphene foam's inner and outer surfaces to prepare a 3D structural gas sensor.[152] The graphene foam provided rich active sites for the absorption of target gas and promoted the formation of p-n heterojunction between N-CDs and TiO_2. Hence, the obtained nanohybrid exhibited excellent sensing properties toward low concentration formaldehyde (HCHO) gas. Specifically, the Au, N-CDs/TiO_2/graphene showed a higher response to HCHO at 150 °C. Moreover, the hybrid sensor still displayed a fast response and recovery for detecting HCHO at ppb level under 90% relative humidity. In another report, Byun et al. fabricated a highly selective NO_2 gas sensor using CDs-modified SWCNTs.[153] The CDs/SWCNTs-based sensor showed high responses to NO_2 gas while weak responses to other gases. Interestingly, the resistance response of this sensor to NO_2 was opposite to previously reported SWCNT-based NO_2 gas sensors. This phenomenon was caused by the doping of SWCNT with electron-rich CDs resulting in the change of polarity from p-type to n-type.

3.2.3. Carbon Dots/Metal Oxide Semiconductor Composites as Sensing Substrates

Metal oxide semiconductors such as SnO_2, In_2O_3, ZnO_2, and TiO_2 are ideal sensing materials for gas sensors attributed to their high sensitivity, simple preparation, and low cost.[154–156] Constructing heterojunctions is a promising approach to enhancing the sensitivity of semiconductor materials because heterojunctions facilitate the expansion of the depletion region and the separation of carriers. CDs, as novel 0D nanomaterials, have many highly reactive surface functional groups, which can modulate the ability of the composites to absorb gas molecules. And the excellent electron transport properties of CDs can regulate the heterojunction carrier reservoirs.[43,157]

As an n-type semiconductor, SnO_2 is considered one of the most promising materials for detecting NO_2 gas. However, high operating temperatures, low response values to low concentration NO_2, and the tendency to agglomerate during preparation limit the application of SnO_2. Thereby, there is a great need for the modification of SnO_2 to improve its performance as a gas sensor. Recently, Li and his colleagues deposited N-CDs uniformly on the surface of SnO_2 via the impregnation-calcination method.[158] The high-resolution TEM characterization indicated that the N-CDs are well decorated on the surface of mesoporous SnO_2 nanosheets (Figure 4b). The fabricated N-CDs modified SnO_2 (N-CDs/SnO_2) sensors exhibited high sensitivity, good selectivity, and excellent stability. Specifically, the response values of N-CDs/SnO_2 sensors for low concentrations (1 ppm) of NO_2 were 2.2 times higher than that of pure SnO_2. Meanwhile, the operating temperature was also reduced to 130 °C.

In_2O_3 has been widely investigated attributed to its wide bandgap and high resistance response to NO_2. Nevertheless, pristine In_2O_3 still possesses some shortcomings, such as limited specific surface area, insufficient active sites, and hindered gas diffusion paths, which resulted in high working temperature and poor selectivity.[159,160] Although various morphologies of In_2O_3 had been successfully synthesized to improve their performance as gas sensors, just as nanoparticles, nanowires, and hollow porous structures,[161,162] the improvements have not yet been satisfactory. Yao et al. constructed nitrogen-doped CDs decorated 3D ordered macroporous (3DOM) In_2O_3 heterojunction materials via template method and hydrothermal treatment (Figure 4c).[163] In comparison with pure 3DOM In_2O_3, the fabricated composite showed better NO_2 sensing properties with a fast speed of response and recovery, low operating temperature (100 °C), excellent NO_2 selectivity, and reduced detection limits (100 ppb). Gao et al. further improved the gas-sensitive performance of gas sensors by using CDs as dopants to decorate hierarchical litchi-like In_2O_3 nanospheres (Figure 4d).[164] The CDs/In_2O_3-based sensors exhibited enhanced response for NO_2 with a theoretical detection limit as low as 9 ppb at a relatively low working temperature (50 °C). It was suggested that the construction of heterojunctions between CDs and In_2O_3 bends the energy band, which broadens the depletion layer. In addition, the introduction of CDs contributes to increasing the number of adsorbed state oxygen and oxygen defects, thus improving the reaction with NO_2.

The 2D materials have emerged as a class of promising materials in various sensing detection due to many advantages, including large specific surface area, abundant oxygen vacancies, more opportunities to contact and react with analyte molecules, and shorter electron transport distances. Loading the 0D nanodots on the 2D nanosheets can further improve the dispersion of the nanoparticles. Therefore, a self-assembly method was developed by Shao's group to prepare novel composite materials (CDs/SnO_2/ZnO) of CDs-modified porous hierarchical SnO_2 quantum nanoparticles and ZnO nanosheets for H_2S detection.[165] The synergistic effect of the p-n heterojunction formed among p-type CDs and n-type SnO_2 and ZnO significantly increased the change in resistance caused by the variation of oxygen adsorption. Compared with pristine ZnO and SnO_2/ZnO sensors, the CDs/SnO_2/ZnO sensor showed higher response values, lower detection limit, faster response speed, and better selectivity. Similarly, the authors fabricated a highly efficient VOCs gas sensor constructed from CDs/TiO_2 films.[166] The obtained composite film exhibited excellent room temperature selectivity of isopropanol vapor, fast response and recovery properties, and stability attributed to their highly ordered nanostructure, larger surface area, and stronger VOCs absorption capacity.

3.2.4. Carbon Dots/Conducting Polymers as Sensing Substrates

Conductive polymers such as polyaniline (PANI), polythiophene, and their derivatives have been extensively investigated as gas sensing materials due to the merits of fast response, low cost, and high selectivity at room temperature. When exposed to different atmospheres, the electronic properties

of conjugated π-bonds along the polymer backbone are significantly changed owing to the interaction between the surface of polymer and gas molecules, leading to the resistance variation.[167] However, some disadvantages of lower response values and poor thermal stability of such materials may be a restriction for practical applications. To solve these issues, Mojtaba et al. innovatively synthesized an S,N-CDs/PANI-based flexible sensor to achieve high response, excellent selectivity, and short response and recovery time to ammonia at room temperature.[168] The introduction of S,N-CDs in PANI resulted in a five-fold improvement of response value than pure PANI at 100 ppm NH_3. Besides, the S,N-CDs/PANI composite sensors showed remarkable responses to ammonia compared to toluene, methanol, acetone, ethanol, chlorobenzene, and propanol vapors. When the hybrid gas sensor gives exposure to NH_3, the combined effects of the deprotonation process of PANI and the electron donor role of S,N-CDs, as well as the extension of electron transfer paths across the PANI chain generated by the swelling process, caused the increase in resistance. In addition, they made a N-CDs modified poly(3,4-ethylenedioxythiophene)-poly(styrenesulfonate) (PEDOT-PSS) gas sensor for VOCs sensing. The experimental results showed that methanol vapor exhibited higher resistance variation than the other organic gases at room temperature. The mechanism of the increase in resistivity could be explained by the decrease in the number of carriers due to the interaction between holes of N-CDs/PEDOT-PSS surface and the electron of methanol. Moreover, the dissolution of methanol in polymer substrates led to the increased distance of polymer interchain and invalidation of N-CDs as conductive pathways.

3.2.5. Other Carbon Dots-Based Composites as Sensing Substrates

Perovskite with semiconducting properties is considered a promising material in the field of gas detection. However, there is still a considerable challenge for practical application to reduce the operating temperature of the perovskite-based sensor. Compared to gas sensors made of pure perovskite, the introduction of CDs can activate the adsorption and desorption of VOCs at room temperature. Therefore, Zhang's group prepared a series of heteroatom-doped CDs to decorate Ag-$LaFeO_3$ (AL) to fabricate hybrid sensors.[169] The results showed that the B-doped CDs exhibited p-type semiconductor behavior and significantly decreased the operating temperature of AL from 90 to 55 °C. In contrast, pure CDs, N-, S-, and Cl- doping CDs raised the AL's working temperature in different degrees. The authors speculated that the more external electrons of the doping atoms, the higher the operating temperature of this composite sensor.

Recently, SiNW has received widespread attention as sensing materials since they combine multiple advantages including easy surface modification, superior surface activity to analytes, and easy compatibility with modern electronic devices. Unfortunately, silicon is easy to be oxidized in contact with corrosive gases, thus the oxide layers can block the carrier transfer path between the silicon and the analyte gas. According to the report of Li's group, they fabricated a novel radial core–shell structural sensor based on the CDs decorated SiNW array to achieve specific identification of NO_2.[170] Compared to the bare SiNW array, the CDs/SiNW composite showed super-high sensitivity of low concentration NO_2 at room temperature and faster response and recovery speed (Figure 4e). Furthermore, the repeatability and stability showed tremendous improvement, and no sensitivity declined after air storage for 2 weeks.

4. Carbon Dots-Based Photocatalysts for Air Pollutants Removal

As mentioned above, CDs-based materials show great potential for air pollutant detection due to their outstanding photoelectric and adsorption properties. However, the problem of efficient elimination of gaseous contaminants from disorganized emissions still needs to be solved. In recent years, extensive reports have demonstrated that semiconductor photocatalysts can degrade a wide range of inorganic and organic pollutants.[183–187] What's more, the functional CDs have also been regarded as promising modifiers that can be utilized for decorating photocatalysts to improve their degradation performance, because of the multiple roles such as accelerating carriers separation, increasing spectral absorption, regulating energy band, and providing adsorption sites.[188] This section will introduce the applications of the CDs-based photocatalysts in photocatalytic degradation of typical inorganic and organic gaseous contaminants (NO_x and VOCs) and explore the mechanism for enhancing the hybrid nanocomposite performance. **Table 2** summarizes the catalytic performance of CDs-based photocatalysts for the degradation of typical air pollutants.

4.1. Carbon Dots-Based Photocatalysts for NO_x Removal

NO_x is mainly derived from the combustion of fossil fuels. It is considered to be the fundamental cause of acid rain and photochemical smog.[189] NO_x contains NO and NO_2, among which the proportion of NO in typical industrial tail gas is about 95% of NO_x.[190] Various effective technologies such as NO_x storage and reduction, selective catalytic reduction (SCR), and selective non-catalytic reduction have been used for NO_x removal.[191–193] However, these approaches are not cost-effective in eliminating NO_x at a ppb level. Photooxidation has gained much attention in recent years as it has immense potential in low concentration NO_x removal. Nonetheless, the photocatalytic efficiency is still limited by the fast electron-hole recombination and low absorption of the solar spectrum of conventional photocatalysts. Moreover, the mechanism of photooxidation of NO follows the process: $NO \rightarrow HNO_2 \rightarrow NO_2 \rightarrow HNO_3$.[194] Once NO oxidation is incomplete, NO_2 will be easily generated, which is more harmful to the environment. Therefore, the ideal photocatalysts are ones with high conversion of NO and low selectivity of NO_2. With the efforts of the researchers, compounding CDs with photocatalysts has been considered to be a promising strategy to solve these problems. For instance, CDs were coupled to nitrogen atom modified $Bi_2O_2CO_3$ (CDs/N-BOC) via impregnation treatment for photocatalytic NO oxidation under visible light. Compared to pristine N-BOC, the removal efficiency of NO increased significantly on CDs/N-BOC, and the

Table 2. Summary of photocatalytic degradation of air pollutants by CDs-based photocatalysts.

Air pollutant	CDs-based photocatalyst	Reactor style	Light source	Light intensity	Wavelength	Initial concentration	Performance	Ref.
O-dichlorobenzene	N-CD/$ZnFe_2O_4$	Batch reactor	500 W Xe lamp	33 mW cm^{-2}.	>400 nm;	5 µL liquid o-dichlorobenzene in reactor (130 mL) to evaporate	74% removal efficiency in 420 min	[226]
Formaldehyde; acetone	CDs/WO_3	Batch reactor	500 W Xe lamp	400 mW cm^{-2}	>420 nm	40 µL of 37 wt% formaldehyde solution (or 20 µL of liquid acetone) to evaporate	411 µmol g^{-1} h^{-1} and 188 µmol g^{-1} h^{-1} CO_2 production rate of formaldehyde and acetone	[206]
Acetaldehyde	CDs/TiO_2	Continuous reactor	65 W fluorescent lamps	20 mW cm^{-2}	>380 nm	500 ppm	99% removal efficiency	[208]
O-xylene	CDs/TiO_2	Continuous reactor	400 W Xe lamp	80 mW cm^{-2}.	>400 nm	50 ppm	87% degradation efficiency	[221]
Toluene	N-CDs/TiO_2	Batch reactor	300 W Xe lamp	612 mW cm^{-2}	350–780 nm	665 ppm	93% mineralization rate in 6 h	[214]
Toluene	CDs/BOC	Batch reactor	300 W Xe lamp		Full spectrum	94.3 ppm	96.62% removal efficiency in 3 h	[227]
Toluene	CDs/BiOCl	Continuous reactor	300 W ultraviolet light		365 nm.	50 ppm	65.4 removal efficiency and 65.2% mineralization efficiency in 1 h	[215]
Acetone	CDs/Bi_2WO_6	Batch reactor	500 W Xe lamp	400 mW cm^{-2}.	>420 nm	5 µL liquid acetone/ toluene in reactor (250 mL) to evaporate	CO_2 production rate : 47 ppm h^{-1}	[209]
Benzene; methanol	CDs/Fe_2O_3	Batch reactor	8 W visble light lamp			15.6 ppm	80% degradation efficiency of benzene in 24 h 70% degradation efficiency of methanol in 24 h	[204]
Benzene; toluene	CDs/CdS/TiO_2	Batch reactor	300 W Xe lamp		Visible light	30 µg mL^{-1}	90% degradation efficiencies for benzene within 1 h and toluene in 2 h	[216]
Benzene, toluene, and *p*-xylene	CDs/TiO_2	Continuous reactor	Xe lamp		UV–vis light	60 ppm (20 ppm benzene + 20 ppm toluene + 20 ppm p-xylene)	64% photodegradation efficiency of mixed VOCs (13%, 64%, 99% photodegradation efficiencies of benzene, *p*-xylene, and toluene.)	[222]
Toluene; formaldehyde	CDs/Bi_2WO_6	Batch reactor	1000 W Xe lamp	200 mW cm^{-2}.	Visible light	350 mg m^{-3}	96.9% degradation efficiencies of toluene and 97.1% degradation efficiencies of formaldehyde in 120 min	[228]
1,3,5-trimethylbenzene; *o*-xylene	NCDs/ $ZnFe_2O_4$/ BiOBr	Continuous reactor	8 W daylight.			1.0 ppm	85.5% and 52.9% photocatalytic efficiency of TMB and XYL	[223]
NO	SnO_2/NCDs/ $ZnSn(OH)_6$	Continuous reactor	1000 W Xe lamp		>420 nm.	400 ppb	37% removal efficiency of NO and NO_2 was suppressed completely	[198]
NO	CDs/$ZnFe_2O_4$	Continuous reactor	300 W Xe lamp	960 mW cm^{-2}.	>420 nm;	400 ppb	38% removal efficiency of NO	[197]

Table 2. Continued.

Air pollutant	CDs-based photocatalyst	Reactor style	Light source	Light intensity	Wavelength	Initial concentration	Performance	Ref.
NO	CDs/FeOOH	Continuous reactor	300 W Xe lamp	28.29 mW cm^{-2}.	>420 nm	400 ppb	22% NO removal efficiency of NO	[229]
NO	SnO_2/CDs	Continuous reactor	100 W tungsten halogen lamp		Full spectrum and visible light	600 ppb	57% and 75% removal efficiency of NO under visible light and full spectrum	[230]
NO	N-CDs/TiO_2	Continuous reactor	12 W ultraviolet lamp	1 mW cm^{-2}. 5 mW cm^{-2}.	Highest emission at 365 nm; >400 nm;	1000 ppb	27% and 79.6% removal efficiency of NO under visible light and UV light	[231]
NO	N-BOC/CDs	Continuous reactor	300 W Xe lamp		>420 nm.	550 ppb	53% removal efficiency of NO	[195]
NO	NCDs/$PrFeO_3$/Pal	Continuous reactor	500 W Xe lamp	50 mW cm^{-2}.	>420 nm;	1000 ppm	93% NO conversion rate, 100% N_2 selectivity, and outstanding resistance to SO_2 and H_2O	[199]
NO	CDs/$CaTiO_3$	Continuous reactor	300 W Xe lamp		>420 nm.	400 ppb	25% removal efficiency of NO	[232]
NO	CDs/TiO_2	Continuous reactor	150 W Xe lamp		420–780 nm.	10 ppm	71% removal efficiency of NO	[233]

selectivity of NO_2 decreased.[195] Furthermore, Cui et al. fabricated CDs/Bi_2WO_6 composite for improving the photocatalytic degradation of NO under simulated sunlight radiation.[196] The conversation rate of NO increased from 19% to 73%, and the selectivity for the formation of NO_x^- raised from 66 to 88% after the incorporation of CDs to Bi_2WO_6. It was found that the Z-scheme heterojunction between CDs and Bi_2WO_6 was the critical factor for the enhanced photocatalytic oxidation of NO.

Huang et al. fabricated a novel CDs/$ZnFe_2O_4$ composite photocatalyst with good biocompatibility and low cytotoxicity, which was obtained via a facile hydrothermal synthesis.[197] With the loading of CDs, the nanohybrid exhibited enhanced photocatalytic performance of NO_x and high selectivity for NO_3^- compared to pristine $ZnFe_2O_4$. It was found that the CDs acted as electron reservoirs and transporter resulting in a higher electron transfer rate and photo-induced carriers separation efficiency of the CDs/$ZnFe_2O_4$. They further fabricated N-CDs decorated mesoporous SnO_2/$ZnSn(OH)_6$ heterojunction for low concentrate NO removal.[198] The NO removal efficiency of the ternary SnO_2/N-CDs/$ZnSn(OH)_6$ (SnO_2/NCDs/ZHS) nanohybrids reached 37%, higher than that of ZSH, SnO_2/ZSH, and NCDs/ZSH, and the toxic NO_2 by-product was suppressed completely. The photocatalytic performance and selectivity were almost unchanged even after the 10-cycle experiment. The reason for the enhanced photocatalytic capability was explored in deep by the authors. The PL emission spectral (**Figure 5**a) indicated that the introduced N-CDs could convert long-wavelength light (550–850 nm) to short-wavelength (300–650 nm), resulting in efficient absorption of the fluorescence emitted from N-CDs to generate charge carriers in the SnO_2/NCDs/ZSH photocatalyst. Furthermore, the significant difference in reactive oxygen species generation from pristine ZHS, NCDs/SnO_2, NCDs/ZHS, and SnO_2/NCDs/ZHS samples implied that the Z-scheme heterogeneous junction was formed between SnO_2/NCDs/ZSH, which changed the transfer pathway of photogenerated carriers and maximized the redox capacity under visible and NIR light, as shown in Figure 5b. Besides, the SnO_2/NCDs/ZSH could provide sufficient free surface ·OH to accelerate the formation of reactive oxygen radicals. More importantly, in situ diffuse reflectance infrared Fourier transform spectroscopy (DRIFTS) revealed the oxidation pathway of NO over SnO_2/NCDs/ZSH ($NO \rightarrow NO^+ \rightarrow NO_2^- \rightarrow NO_3^-$), which provided rigorous evidence for the conversion of NO into major harmless final products and inhibition of toxic by-product.

Compared to the photooxidation strategy for low concentration NO_x removal, photocatalysis-selective catalytic reduction (photo-SCR) can eliminate high concentrations NO_x. Li and co-authors synthesized a hybrid structure of N-CDs-modified $PrFeO_3$/palygorskite (NCDs/$PrFeO_3$/Pal) via the sol-gel-impregnation method for photo-SCR of NO_x.[199] With the optimum loading amount of N-CDs (5 wt%), NCDs/$PrFeO_3$/Pal was found to present the highest conversion efficiency of 93% and 100% N_2 selectivity. Additionally, the water and sulfur resistance of composite photocatalyst showed significant improvement compared to pristine $PrFeO_3$/Pal (Figure 5c). This was mainly because the introduction of N-CDs favored the adsorption of SO_2 and H_2O, thus preventing NH_3 from being sulfated by SO_2 and the photocatalyst from being corroded by H_2O.

4.2. Carbon Dots-Based Photocatalysts for Volatile Organic Compounds Removal

VOCs, one of the most common types of air pollutants, include alcohols, aldehydes, ketones, and aromatics (benzene, toluene, xylene, etc.). A large number of studies have reported on VOCs

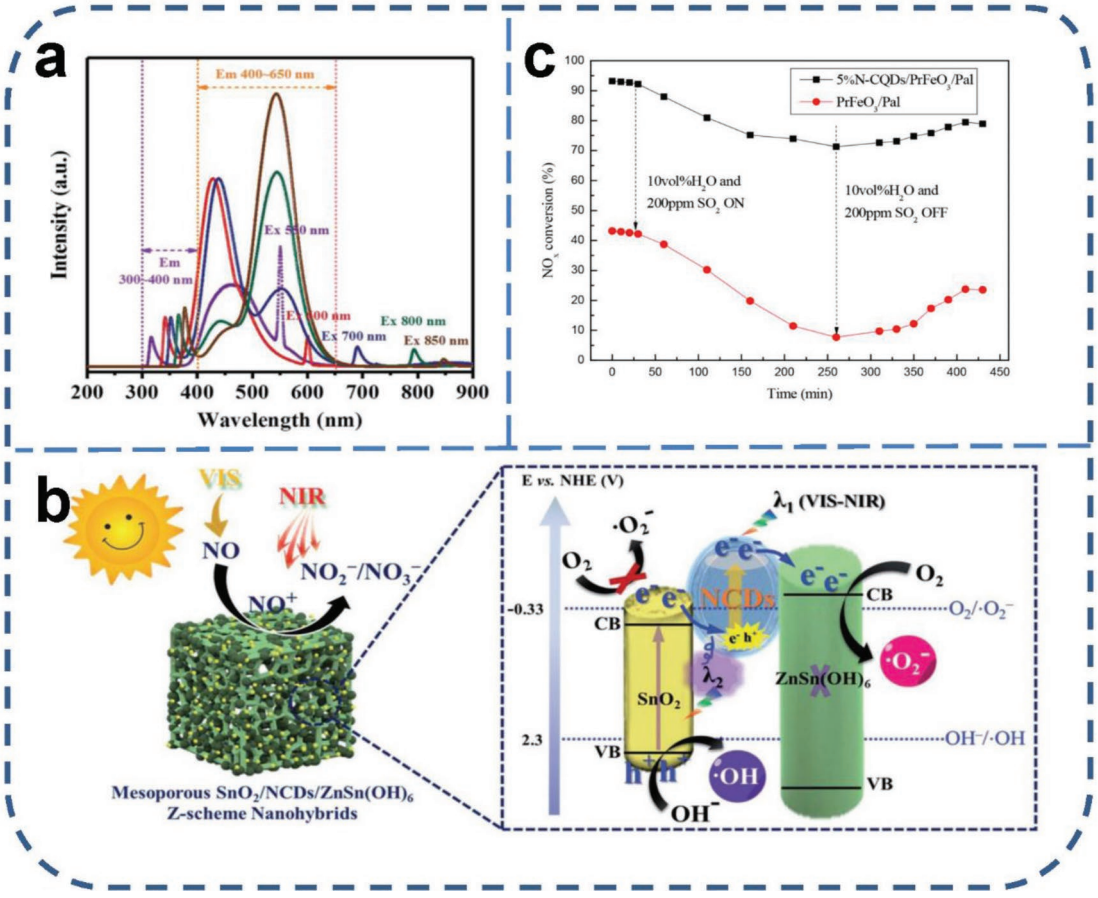

Figure 5. a) Fluorescence spectra of N-CDs at different excitation light wavelengths. b) Photocatalytic conversion route and the reaction mechanism of NO on the surface of the SnO_2/NCDs/ZHS nanocomposite under vis–NIR irradiation. Reproduced with permission.[198] Copyright 2019, Royal Society of Chemistry. c) Effect of SO_2 and H_2O on the NO_x conversion over $PrFeO_3$/Pal and N-CDs/$PrFeO_3$/Pal catalysts. Reproduced with permission.[199] Copyright 2018, American Chemical Society.

photocatalytic oxidation using wide bandgap semiconductor photocatalysts such as TiO_2-based and Bi-based nanocomposites.[184,200–202] However, poor light adsorption and the high recombination of photogenerated carriers limited their practical usage. Recently, CDs-based photocatalysts have been increasingly investigated for the removal of different types of VOCs. The specific applications and mechanisms are described below.

4.2.1. Alcohols

Alcohol is normally added to cosmetics and skincare products. Long-term exposure to short-chain alcohols (methanol, ethanol) can cause a narcotic effect on the central nervous system and damage the optic nerve and retina.[203] Zhang et al. first synthesized CDs/Fe_2O_3 nanohybrids to investigate their photodegradation activity of gaseous methanol.[204] After 25 h of visible light illumination, the photocatalytic efficiency of CDs/Fe_2O_3 on methanol reached 70%, while that of pristine Fe_2O_3 was just 50%. The introduction of CDs onto Fe_2O_3 particles produced three effects: 1) CDs could be used as an electron storage layer to capture the electrons excited from Fe_2O_3 under irradiation, thereby hindering the recombination of photogenerated carriers. 2) The reactive superoxide radicals could be formed on the surface of CDs by the reaction between absorbed O_2 and the transferred electron from Fe_2O_3. 3) The up-conversion photoluminescence property of CDs enabled Fe_2O_3 to produce more electrons and holes, which in turn improved the photocatalytic ability of the composite. The photocatalytic process of CDs/Fe_2O_3 was shown in **Figure 6**a.

4.2.2. Aldehydes

Aldehydes are one of the most prevalent indoor air pollutants. Formaldehyde and acetaldehyde are two common substances that are usually released from building materials and pose a threat to human health. Xu's group studied the photocatalytic removal of formaldehyde by a series of CDs/Bi_2WO_6 (CBW) composites under visible light, wherein CDs were synthesized from different precursors including chitosan, glucose, L-ascorbic, sucrose, and citric acid.[205] The results showed that all the CBW hybrids exhibited superior photocatalytic performance than that of pure Bi_2WO_6. In particular, the CBW derived from chitosan (C-CBW) displayed the highest catalytic activity with 96.7% degradation efficiency for gaseous formaldehyde within 120 min.

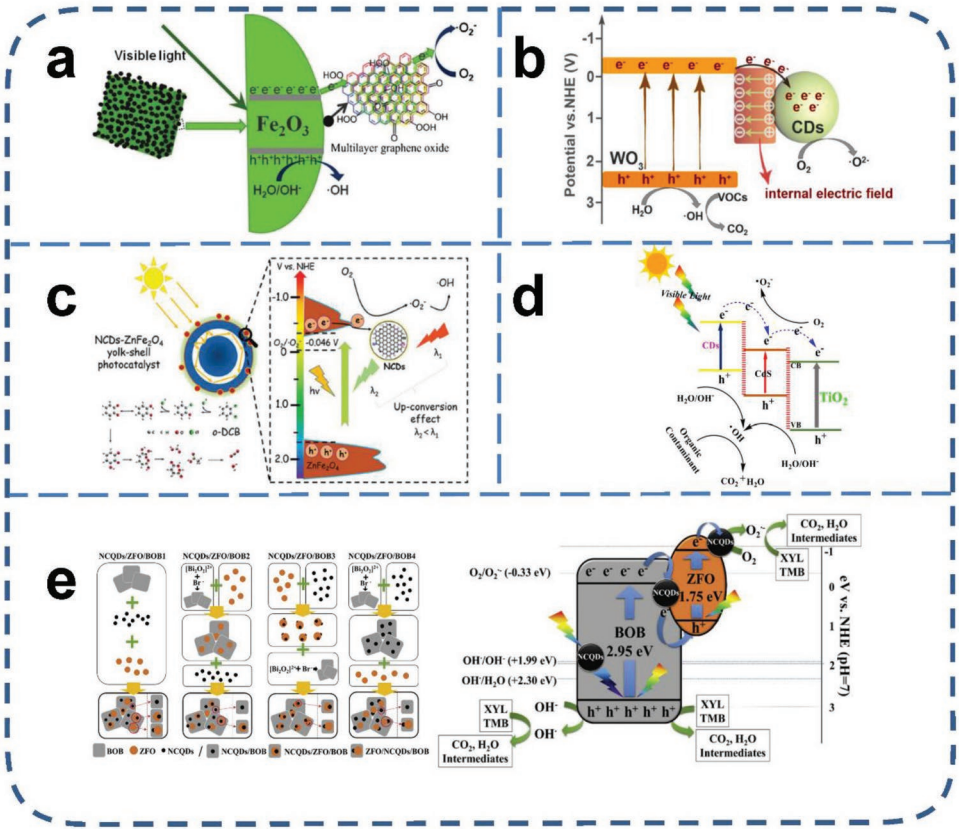

Figure 6. a) Schematic representation of photodegradation gaseous methanol by Fe_2O_3/CDs composites under visible light. Reproduced with permission.[204] Copyright 2011, Royal Society of Chemistry. b) Schematic sketch of the carriers' separation of CDs/WC during photocatalytic degradation of formaldehyde. Reproduced with permission.[206] Copyright 2021, Elsevier. c) Illustration of *o*-DCB photodegradation pathway on the N-CDs/$ZnFe_2O_4$ yolk-shell nanohybrid under visible light irradiation. Reproduced with permission.[226] Copyright 2019, Royal Society of Chemistry. d) Schematic illustration of charge transfer and separation on CDs/TiO_2/CdS ternary photocatalyst under visible-light irradiation. Reproduced with permission.[216] Copyright 2018, Elsevier. e) Schematic illustration of the synthesis processes and structures for different junctions between N-doped CDs, $ZnFe_2O_4$, and BiOBr (left), and the mechanism diagram of photocatalytic removal of TMB and XYL upon NCDs/ZFO/BOB1 (right). Reproduced with permission.[223] Copyright 2019, Elsevier.

From a series of optical properties characterization, the C-CBW possessed the widest absorption band, best carrier separation capability, and fastest electron migration rate. Most recently, novel CDs modified WO_3 nanoplates (CW) for photodegradation of formaldehyde was fabricated.[206] The CW composite showed a remarkable photocatalytic capability with a CO_2 production rate of 411 μmol g^{-1} h^{-1}, exceeding most of the photocatalysts that have been reported in other literature. The authors demonstrated that an interfacial electric field (IEF) was built at the interface between CDs and WO_3 by using theoretical calculations and in situ XPS, which enabled the effective separation of photogenerated carriers. The specific mechanism was described in Figure 6b. The IEF with direction pointing from CDs to WO_3 was formed due to the different work functions between CDs and WO_3. Under visible light irradiation, valence band electrons of WO_3 were excited to leap to the conduction band. Followed driven by IEF, the photoexcited electrons at the conduction band of WO_3 migrated to CDs, while holes stayed at the valance band of WO_3, thus achieving efficient electron-hole separation. Subsequently, the separated carriers participated in redox reactions with O_2 and H_2O on the surface of CW to form active radicals, eventually mineralizing formaldehyde to CO_2.

Acetaldehyde, another highly reactive aldehyde, not only poses a threat to human health because of its cytotoxic and carcinogenic properties, but also readily reacts with O_3, NO_x, and other active gases in further rearrangements.[207] TiO_2 is most widely used in the photodegradation of acetaldehyde, but wide bandgap (≈3.2 eV) and low utilization of the solar spectrum limit its application. Hu et al. proposed a promising strategy to couple CDs with TiO_2 to expand the optical absorption band of CDs/TiO_2 to the visible light region.[208] Surprisingly, the fabricated composite photocatalyst showed excellent photocatalytic performance with 99% removal efficiency of acetaldehyde, while the degradation efficiency of pure TiO_2 was just 46%. The improved photocatalytic performance could be attributed to the introduction of CDs facilitating the formation of Ti^{3+} defective energy level and promoting the CDs/TiO_2 to adsorb acetaldehyde, thus narrowing the bandgap and improving the contact with the target gas.

4.2.3. Ketone

Ketone is a compound in which a carbonyl group is attached to two hydrocarbon groups. Gaseous ketones are mainly derived

from the volatilization of varnishes, paints, and adhesives. Acetone is the most widely used model compound in the investigations of photocatalytic oxidation of gaseous ketones. Zhao's group incorporated CDs with Bi_2WO_6 via a facile wet impregnation method for photocatalytic degradation of acetone vapor.[209] The as-synthesized catalysts extended the light absorption into the visible light region and promoted the efficiency of photoexcited charge separation. CDs/Bi_2WO_6 with 4 g of CDs stock solution displayed the highest CO_2 production rate, achieving 48 ppm h^{-1} within 8 h. In addition, CDs/Bi_2WO_6 also exhibited excellent stability and durability after conducting four consecutive photo-degradation cycles.

4.2.4. Aromatic Hydrocarbons

Aromatic hydrocarbons are a class of typical gaseous pollutants, including benzene, toluene, xylene, trimethylbenzene, etc. They originate from various sources, such as car exhaust, organic solvents in buildings, and decoration materials. Because of the high photochemical reactivity in the atmosphere, aromatic hydrocarbons could promote the formation of atmospheric photo-oxidants (e.g., ozone and peroxyacetyl nitrate) and secondary organic aerosols, thus producing greater harm to human health.[210–212] Therefore, the removal of aromatic hydrocarbons from the air is essential.

In earlier years, benzene was extensively employed in adhesives and paints as an organic solvent. Considering benzene's carcinogenic properties, it has been substituted by the comparatively less harmful toluene.[213] Therefore, the photocatalytic removal of toluene has received increasing attention. However, the most prominent problem in the photodegradation of aromatic hydrocarbons is the deactivation of the photocatalyst due to the deposition of intermediates on the catalyst surface as a result of low mineralization rates. According to the report from Yu et al., they prepared N-CDs/TiO_2 nanomaterials for photodegradation toluene, which exhibited a mineralization rate of 93% under simulated sunlight irradiation for 6 h, while that of commercial photocatalyst TiO_2 (P25) was just 37%.[214] In another report, novel photocatalysts of CDs/BiOCl exhibited nearly three times the toluene mineralization efficiency of pristine BiOCl.[215] The authors used theoretical calculations to investigate the adsorption process of toluene oxidation intermediates on different photocatalysts' surfaces. The adsorption energies of toluene oxidation intermediates on the surface of CDs/BiOCl were lower than that of BiOCl, which indicated the addition of CDs could promote the selective conversion of toluene to benzoic thus facilitating the ring-opening reactions and achieving the complete oxidation of toluene. Moreover, the experimental results of in situ DRIFTS verified this inference. Yang's group conducted comparative research on benzene and toluene photodegradation using ternary CDs/TiO_2/CdS photocatalyst.[216] The fabricated nanohybrids showed 90% photodegradation efficiency for benzene within 1 h and toluene in 2 h, respectively. The experimental results showed that toluene was more difficult to degrade than benzene, which was consistent with other literature reports.[217–219] Surprisingly, the introduction of CDs reduced the CdS quantum dots' photo corrosion and contributed to the formation of photoexcited electron transfer pathways from CDs to CdS (Figure 6d), thus leading to a high separation rate between photoinduced electron-hole pairs and the generation of superoxide radicals.

Some research has shown that the TiO_2 (001) facet contains under-coordinate Ti and O atoms, which are more reactive for photooxidation.[220] Accordingly, Asad Mahmood et al. synthesized a hybrid structure of CDs decorated TiO_2 nanoparticles with a dominant (001) crystal plane for photocatalytic degradation of *o*-xylene.[221] With loading 1 wt% of CDs, the CDs/TiO_2 showed 87% degradation efficiency of *o*-xylene, 55.3% higher than that of pure TiO_2. The addition of CDs on the TiO_2 surface enhanced the adsorption of *o*-xylene and accelerated the separation of photogenerated carriers. Besides, the FTIR spectral peaks of CO_2 increased in CDs/TiO_2 compared to pure TiO_2, indicating that the addition of CDs promoted the trend of converting *o*-xylene to CO_2 on TiO_2. The authors further researched the potential use of CDs/TiO_2 in photocatalytic degradation of mixed gaseous pollutants containing aromatic rings, including benzene, toluene, and *p*-xylene.[222] With 0.5 wt% CDs modified TiO_2, 64% of the mixed VOCs were degraded. Specifically, the photodegradation efficiency of benzene, toluene, and *p*-xylene was 31%, 64%, and 99%, respectively. The order of ease of photodegradation was consistent with the sequence of adsorption energies of benzene, *p*-xylene, and toluene calculated by the DFT method. Furthermore, the DFT confirmed that the new energy states of the CDs skeleton induced by C_{2p} orbits enhanced the electron-hole separation and light absorption properties of CDs/TiO_2. Recently, Seoung-Rae et al. synthesized three-component photocatalysts with different junctions consisting of N-doped CDs, $ZnFe_2O_4$, and BiOBr (NCDs/ZFO/BOB) to research the influence of heterojunction structure on photocatalytic performance in the degradation of organic gases 1,3,5-trimethyl benzene (TMB) and *o*-xylene (XYL) (Figure 6e).[223] The NCDs/ZFO/BOB1 showed the highest photocatalytic efficiencies of TMB (94.5%) and XYL (72.5%), respectively. The N-CDs in NCDs/ZFO/BOB1 acted as electron mediators to construct the Z-type charge transfer pathways between ZFO and BOB, and enhanced the up-conversion PL performance of NCDs/ZFO/BOB1.

Chlorine-containing volatile organic compounds (CVOCs) are widely emitted from industrial facilities and domestic waste incineration. Serving as an important precursor of dioxins, one of the most toxic CVOCs, *o*-dichlorobenzene (*o*-DCB) is often used as a model CVOCs to explore suitable catalysts.[224,225] Li et al. synthesized a new type of N-CDs decorated $ZnFe_2O_4$ eggshell nanostructure photocatalyst by simple hydrothermal treatment.[226] With the optimum loading amount of N-CDs (3 wt%), N-CDs/$ZnFe_2O_4$ exhibited 74% degradation efficiency for gaseous *o*-DCB in 420 min under visible light. The nanocomposites showed both wide spectral absorption and low carrier recombination rate combined with UV–vis diffuse reflectance spectroscopy and PL emission spectroscopy. The yolk-shell structure of $ZnFe_2O_4$ shortened the migration path of photoinduced carriers and enhanced light scattering between shell layers. DFT calculations further proved that the electrons are more inclined to move from $ZnFe_2O_4$ to N-CDs, thus inhibiting the recombination of photogenerated electrons and holes. Furthermore, in situ FTIR and electron paramagnetic

resonance revealed the catalytic path and reactive species in the photodegradation process. The probable mechanism for *o*-DCB degradation was illustrated in Figure 6c.

4.3. Computational Studies

The above-mentioned extensive experimental reports suggest that the composite of CDs with semiconductor photocatalysts can further enhance photocatalytic performance. Meanwhile, these experimental results are also supported by theoretical calculations. DFT-based computational modeling methods are used to investigate structural, electronic, and chemical properties of CDs and their nanocomposites, such as electron transfer processes, structural steady states, ease of adsorption with reactants, and reaction intermediate processes.[53,228,229] Cui et al. used theoretical calculations to study the electron leap and energy level change of CDs and Bi_2WO_6 in the process of forming composite photocatalysts.[196,197] The electron density difference and Bader charge calculated by DFT indicated that the CDs received electrons during the process of adsorption onto the Bi_2WO_6 surface (**Figure 7**a). Moreover, the density-of-state peaks showed that the addition of CDs led to a slight reduction of the bandgap and enabled the electrons from the conduction band of Bi_2WO_6 to the valence band of CDs, as shown in Figure 7b,c. This was consistent with the experimental

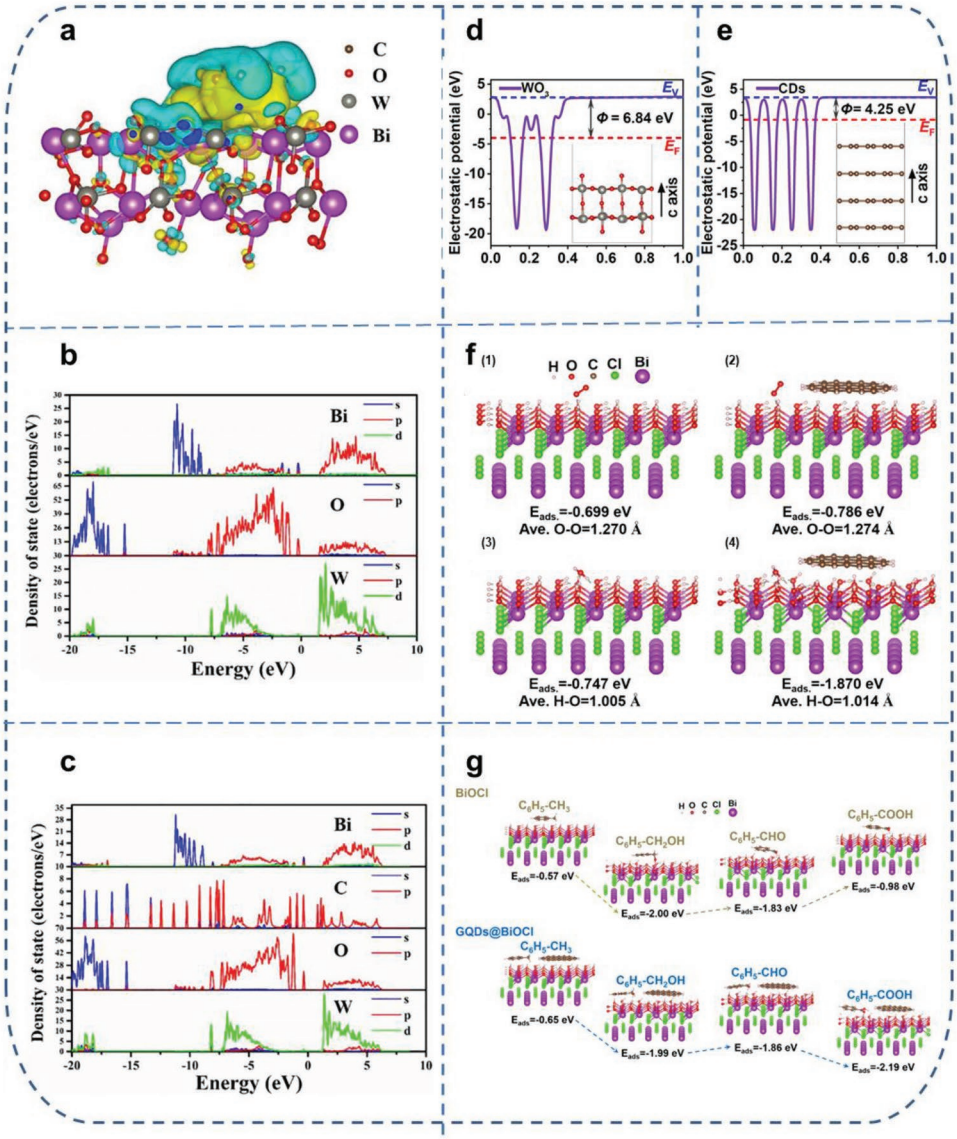

Figure 7. a) Side view of electron density difference of CDs/Bi_2WO_6. b) DOS of Bi, W, O elements of Bi_2WO_6 supercell. c) DOS of Bi, C, O, W elements of CDs/Bi_2WO_6. Reproduced with permission.[196] Copyright 2021, Elsevier. d) Static electronic potentials of WO_3 (001) slab. e) Static electronic potentials of CDs (001) slabs. Reproduced with permission.[206] Copyright 2021, Elsevier. f) Simulated adsorption process: 1) O_2 adsorption on BiOCl nanosheets. 2) O_2 adsorption on CDs/BiOCl heterojunction. 3) H_2O adsorption on BiOCl nanosheets. 4) H_2O adsorption on CDs/BiOCl heterojunction. g) Schematic diagram of the theoretical calculation of adsorption energy (E_{ads}) of each intermediate in the photocatalytic toluene process over BiOCl and CDs/BiOCl. Reproduced with permission.[215] Copyright 2021, Elsevier.

result that Z-type heterojunctions were formed between CDs and Bi_2WO_6. Similarly, Huang et al. fabricated a nanocomposite CDs/WO_3 for photooxidation of formaldehyde and acetone.[206] The DFT study calculated work function (ϕ) of WO_3 and CDs were 6.84 and 4.25 eV, respectively, as shown in Figure 7d,e. As a result, some electrons in CDs would transfer to WO_3 upon their hybridization until their Fermi energies reached the same level. As the positive and negative charges accumulated on WO_3 and CDs, an internal electric field was formed that facilitated the charge separation. In another research of the photodegradation of toluene over CDs/BiOCl nanosheets, the authors calculated the adsorption energies and bond lengths of O_2 and H_2O molecules on the surfaces of pristine materials and heterojunctions by DFT, as displayed in Figure 7f.[215] The results indicated that the O_2 and H_2O molecules were more readily adsorbed and activated to generate $\cdot O^-_2$ and $\cdot OH$ radicals on the heterojunction surface than on the pure BiOCl surface. Besides, the oxidation process of toluene was deduced from the results of the adsorption energies of toluene and its intermediates calculated by DFT, as shown in Figure 7g. The calculated toluene open-loop path was consistent with the in situ characterization results. Especially, the calculation results illustrated that the enhancement of the toluene mineralization rate is due to the introduction of CDs to improve the adsorption and activation of benzoic acid on the surface of the composite photocatalyst. Based on extensive experimental and theoretical analysis, it can be proved that CDs are a highly promising material for air purification.

5. Conclusions and Outlook

The emergent CDs possess numerous unique features such as environmentally friendly, easily derived from small-molecule chemicals or macroscopic carbon sources, and tunable optical and electronic properties, which made them distinguishable from conventional semiconductors or other carbon nanomaterials. The excellent performance of CDs for gaseous pollutants sensing and photocatalytic removal indicates they can play an increasingly important role in solving atmospheric pollution problems. In particular, CDs' multiple response mechanisms to air contaminants provide more options for developing efficient and easy-to-operate sensors, while their high utilization of solar energy is expected to provide a sustainable approach to air environment remediation. Although the great progress of CDs in the synthesis and performance, the research on air environment monitoring and treatment of CDs-based functional materials is still in the early stage. Herein, several important challenges and bottlenecks are still to be overcome.

One of the most fundamental issues is the controlled large-scale synthesis of high-quality CDs with specific morphologies and surface states. Despite a large number of methods and carbon sources are utilized to synthesize CDs, these methods reported in the literature are unable to balance the high yield of CD with the controllable morphology. Specifically, although the synthetic approaches deprived from bottom-up strategy are simple and inexpensive, the synthesized CDs tend to have large size distributions and uncontrollable structures. While CDs obtained from top-down methods have more concentrated size distributions but lower yields and often require harsh reaction conditions, possibly limiting their wide application. The difficulty of controlled synthesis lies in the lack of comprehension of the relationship -between synthesis methods and structure and properties of CDs. Therefore, it is necessary to use in situ characterization techniques to further understand the formation mechanism of CDs in the synthesis process. In addition, the development of efficient methods to separate CDs based on size, polarity, and shape is urgently demanded.

In the area of air pollutants detection, the CDs-based sensors can be used for sensitive detection of gaseous pollutants by interacting with toxic gas molecules to generate specific optical or electrical signals. However, the optical and electric performance of CDs are susceptible to the external environment and the interference from non-target analytes may affect the specificity of gaseous contaminants detection. From the perspective of practical application, further developments are needed to enhance the selectivity and robustness of CDs-based sensors to detect individual gaseous contamination components in multi-pollutants environments. To achieve these objectives, research needs to be conducted in the following aspects: 1) Combining the physicochemical properties of the target pollutants, CDs can be grafted with functional groups in a targeted manner to increase the specific recognition sites for pollutants or be surface passivated to reduce the adsorption of non-target molecules. 2) Compounding with other porous materials with selective adsorption such as molecular sieves, metal-organic frameworks, and covalent organic frameworks to enhance the response signal of CDs through gas enrichment. In order to analyze multiple pollutants in complex environments, the multi-analyte device that can integrate a series of CDs-based sensors need to be developed. Each CDs-based sensing array will give a response to a specific gaseous pollutant. Moreover, the miniaturization of sensing devices can greatly enhance the accessibility and practicality of monitoring airborne contaminants in real-world scenarios.

As for photocatalytic removal of gaseous pollutants, numerous investigations have demonstrated that CDs can function as electron acceptors or donors to provide alternative electron transfer paths by tuning the energy band alignment between the CDs and the semiconductor, thus improving the separation of photogenerated carriers and increasing the total number of carriers available for the photocatalytic reactions. Nonetheless, the compounding process of CDs with semiconductor photocatalysts is generally carried out in the aqueous phase, and the easy agglomeration property of CDs inevitably affects their dispersion on the catalyst surface, thus reducing the number of active sites. Therefore, it is critical to developing compounding methods with high dispersion to improve the photocatalyst performance and the utilization of CDs. It is worth mentioning that using in situ epitaxial growth strategy is an effective way to achieve homogeneous compounding of CDs with 2D photocatalysts.[234] On the other hand, the CDs' up-conversion PL properties allow them to be a secondary light source for excitation of wide bandgap photocatalysts after combining with other semiconductors. However, the efficiency of up-conversion still needs to be significantly improved for most photocatalytic applications. In addition, the mechanism of

up-conversion luminescence of CDs in photocatalytic systems is still controversial, and more detailed studies on this phenomenon are required.

Compared with the photocatalytic reaction that takes place in the liquid phase, the gas-solid phase photocatalytic reaction is more likely to cause the accumulation of intermediate products on the catalyst surface, even resulting in the deactivation of the catalyst. Meanwhile, the incomplete oxidation products of NO_x such as NO_2 and by-products of VOCs like O_3 are likely to cause more serious secondary pollution. Therefore, the diffusion capacity of gas molecules on the catalyst surface and the oxidation capacity of the catalyst needs to be further improved. Strengthening the following research is expected to achieve these goals: 1) To explore the light-induced electron transfer path, surface adsorption, and activation process of reactive molecules, and understand the relationship between structure and electronic energy levels by theoretical calculations, thus providing theoretical guidance for the rational design of CDs-based photocatalysts with higher activity, selectivity, and stability. 2) Modification of the surface states of CDs by heteroatom doping and functional groups grafting to enhance adsorption and selective removal of target reactant molecules. 3) By tuning the energy band of the CDs to match the energy band of the semiconductor photocatalyst with porous morphology, the photo-redox ability of composite catalysts and the desorption of reaction products can be maximized.

Although the above issues have not been fully addressed, the integration of CDs in sensors or compounding with other photocatalysts has shown great potential for rapid detection and efficient removal of gaseous pollutants. With improved understanding of structure-property relationships of CDs system and enhancing the design and synthesis of CDs, we believe that the CDs-based materials will offer a meaningful route to improve air quality.

Acknowledgements

This work was financially supported by the Key Research and Development Program of Hunan Province in China (2018SK2032) and the National Key Research and Development Program of China (2016YFC0204100).

Conflict of Interest

The authors declare no conflict of interest.

Keywords

air pollutants detection and removal, carbon dots, sensing mechanisms, sensors and photocatalysts fabrication

Received: February 3, 2022
Revised: April 7, 2022
Published online:

[1] J. L. Adgate, B. D. Goldstein, L. M. McKenzie, *Environ. Sci. Technol.* **2014**, *48*, 8307.
[2] E. Webb, J. Hays, L. Dyrszka, B. Rodriguez, C. Cox, K. Huffling, S. Bushkin-Bedient, *Rev. Environ. Health* **2016**, *31*, 225.
[3] X. Tang, P. K. Misztal, W. W. Nazaroff, A. H. Goldstein, *Environ. Sci. Technol.* **2016**, *50*, 12686.
[4] S. S. Schiffman, C. M. Williams, *J. Environ. Qual.* **2005**, *34*, 129.
[5] T. Salthammer, S. Mentese, R. Marutzky, *Chem. Rev.* **2010**, *110*, 2536.
[6] J. Chen, R. Liu, Y. Gao, G. Li, T. An, *J. Cleaner Prod.* **2017**, *148*, 268.
[7] T. An, Y. Huang, G. Li, Z. He, J. Chen, C. Zhang, *Environ. Int.* **2014**, *73*, 186.
[8] A. Azzouz, K. Vikrant, K.-H. Kim, E. Ballesteros, T. Rhadfi, A. K. Malik, *TrAC, Trends Anal. Chem.* **2019**, *118*, 502.
[9] T. A. Saleh, *Environ. Technol. Innovation* **2020**, *20*, 101067.
[10] T. A. Saleh, *Environ. Technol. Innovation* **2021**, *24*, 101821.
[11] D. Xia, H. Liu, B. Xu, Y. Wang, Y. Liao, Y. Huang, L. Ye, C. He, P. K. Wong, R. Qiu, *Appl. Catal. B* **2019**, *245*, 177.
[12] S. N. Baker, G. A. Baker, *Angew. Chem., Int. Ed.* **2010**, *49*, 6726.
[13] S. Zhu, Y. Song, X. Zhao, J. Shao, J. Zhang, B. Yang, *Nano Res.* **2015**, *8*, 355.
[14] H. Choi, S.-J. Ko, Y. Choi, P. Joo, T. Kim, B. R. Lee, J.-W. Jung, H. J. Choi, M. Cha, J.-R. Jeong, *Nat. Photonics* **2013**, *7*, 732.
[15] R. Atchudan, T. N. J. I. Edison, D. Chakradhar, S. Perumal, J.-J. Shim, Y. R. Lee, *Sens. Actuators, B* **2017**, *246*, 497.
[16] N. Dhenadhayalan, K. C. Lin, T. A. Saleh, *Small* **2020**, *16*, 1905767.
[17] Q. He, S. Zhuang, Y. Yu, H. Li, Y. Liu, *Anal. Chim. Acta* **2021**, *1174*, 338743.
[18] J. Wang, Y. Yang, G. Sun, M. Zheng, Z. Xie, *Environ. Res.* **2019**, *177*, 108621.
[19] L. Jia, R. Chen, J. Xu, L. Zhang, X. Chen, N. Bi, J. Gou, T. Zhao, *J. Hazard. Mater.* **2021**, *413*, 125296.
[20] M. Wang, M. Hu, J. Liu, C. Guo, D. Peng, Q. Jia, L. He, Z. Zhang, M. Du, *Biosens. Bioelectron.* **2019**, *132*, 8.
[21] X. Yan, Y. Song, C. Zhu, H. Li, D. Du, X. Su, Y. Lin, *Anal. Chem.* **2018**, *90*, 2618.
[22] X. Wu, Y. Song, X. Yan, C. Zhu, Y. Ma, D. Du, Y. Lin, *Biosens. Bioelectron.* **2017**, *94*, 292.
[23] M. H. M. Facure, R. Schneider, L. A. Mercante, D. S. Correa, *Environ. Sci.: Nano* **2020**, *7*, 3710.
[24] C. Long, Z. Jiang, J. Shangguan, T. Qing, P. Zhang, B. Feng, *Chem. Eng. J.* **2021**, *406*, 126848.
[25] S. Dolai, S. K. Bhunia, S. Rajendran, V. UshaVipinachandran, S. C. Ray, P. Kluson, *Crit. Rev. Solid State Mater. Sci.* **2020**, *46*, 349.
[26] L. Wang, S. Zhu, T. Lu, G. Zhang, J. Xu, Y. Song, Y. Li, L. Wang, B. Yang, F. Li, *J. Mater. Chem. B* **2016**, *4*, 4913.
[27] S. Qu, D. Zhou, D. Li, W. Ji, P. Jing, D. Han, L. Liu, H. Zeng, D. Shen, *Adv. Mater.* **2016**, *28*, 3516.
[28] A. R. Chowdhuri, T. Singh, S. K. Ghosh, S. K. Sahu, *ACS Appl. Mater. Interfaces* **2016**, *8*, 16573.
[29] P. Namdari, B. Negahdari, A. Eatemadi, *Biomed. Pharmacother.* **2017**, *87*, 209.
[30] R. P. Choudhary, S. Shukla, K. Vaibhav, P. B. Pawar, S. Saxena, *Mater. Res. Express* **2015**, *2*, 095024.
[31] P. Tian, L. Tang, K. S. Teng, S. P. Lau, *Mater. Today Chem.* **2018**, *10*, 221.
[32] B. van Dam, H. Nie, B. Ju, E. Marino, J. M. J. Paulusse, P. Schall, M. Li, K. Dohnalová, *Small* **2017**, *13*, 1702098.
[33] C.-Y. Teng, B.-S. Nguyen, T.-F. Yeh, Y.-L. Lee, S.-J. Chen, H. Teng, *Nanoscale* **2017**, *9*, 8256.
[34] M. Shamsipur, A. Barati, S. Karami, *Carbon* **2017**, *124*, 429.
[35] S. Zhou, H. Xu, W. Gan, Q. Yuan, *RSC Adv.* **2016**, *6*, 110775.
[36] J. Valenta, *Nanosci. Methods* **2014**, *3*, 11.
[37] Y. Wang, A. Hu, *J. Mater. Chem. C* **2014**, *2*, 6921.
[38] K. J. Mintz, Y. Zhou, R. M. Leblanc, *Nanoscale* **2019**, *11*, 4634.
[39] S. Lu, G. Xiao, L. Sui, T. Feng, X. Yong, S. Zhu, B. Li, Z. Liu, B. Zou, M. Jin, *Angew. Chem.* **2017**, *129*, 6283.
[40] C. Liu, G. Xiao, M. Yang, B. Zou, Z. L. Zhang, D. W. Pang, *Angew. Chem., Int. Ed.* **2018**, *57*, 1893.

[41] X. Niu, Y. Li, H. Shu, J. Wang, *Nanoscale* **2016**, *8*, 19376.
[42] C. Wang, Z. Xu, H. Cheng, H. Lin, M. G. Humphrey, C. Zhang, *Carbon* **2015**, *82*, 87.
[43] X. Wang, L. Cao, F. Lu, M. J. Meziani, H. Li, G. Qi, B. Zhou, B. A. Harruff, F. Kermarrec, Y.-P. Sun, *Chem. Commun.* **2009**, 3774.
[44] L. Lin, S. Zhang, *Chem. Commun.* **2012**, *48*, 10177.
[45] H. Li, X. Zhang, D. R. MacFarlane, *Adv. Energy Mater.* **2015**, *5*, 1401077.
[46] Y. Yan, J. Gong, J. Chen, Z. Zeng, W. Huang, K. Pu, J. Liu, P. Chen, *Adv. Mater.* **2019**, *31*, 1808283.
[47] M. Han, S. Zhu, S. Lu, Y. Song, T. Feng, S. Tao, J. Liu, B. Yang, *Nano Today* **2018**, *19*, 201.
[48] Y. Ma, X. Li, Z. Yang, S. Xu, W. Zhang, Y. Su, N. Hu, W. Lu, J. Feng, Y. Zhang, *Langmuir* **2016**, *32*, 9418.
[49] H. Fei, R. Ye, G. Ye, Y. Gong, Z. Peng, X. Fan, E. L. G. Samuel, P. M. Ajayan, J. M. Tour, *ACS Nano* **2014**, *8*, 10837.
[50] X. T. Zheng, A. Ananthanarayanan, K. Q. Luo, P. Chen, *Small* **2015**, *11*, 1620.
[51] W. Wu, L. Zhan, W. Fan, J. Song, X. Li, Z. Li, R. Wang, J. Zhang, J. Zheng, M. Wu, H. Zeng, *Angew. Chem., Int. Ed. Engl.* **2015**, *54*, 6540.
[52] J. Feng, H. Dong, L. Yu, L. Dong, *J. Mater. Chem. C* **2017**, *5*, 5984.
[53] D. Saini, A. K. Garg, C. Dalal, S. R. Anand, S. K. Sonkar, A. K. Sonker, G. Westman, *ACS Appl. Nano Mater.* **2022**, *5*, 3087.
[54] H. Yu, R. Shi, Y. Zhao, G. I. Waterhouse, L. Z. Wu, C. H. Tung, T. Zhang, *Adv. Mater.* **2016**, *28*, 9454.
[55] M. R. Pacquiao, M. D. G. de Luna, N. Thongsai, S. Kladsomboon, P. Paoprasert, *Appl. Surf. Sci.* **2018**, *453*, 192.
[56] X. Wang, G. Sun, P. Routh, D.-H. Kim, W. Huang, P. Chen, *Chem. Soc. Rev.* **2014**, *43*, 7067.
[57] R. Xie, Z. Wang, W. Zhou, Y. Liu, L. Fan, Y. Li, X. Li, *Anal. Methods* **2016**, *8*, 4001.
[58] H. Yin, H. Tang, D. Wang, Y. Gao, Z. Tang, *ACS Nano* **2012**, *6*, 8288.
[59] H. Choi, S.-J. Ko, Y. Choi, P. Joo, T. Kim, B. R. Lee, J.-W. Jung, H. J. Choi, M. Cha, J.-R. Jeong, I.-W. Hwang, M. H. Song, B.-S. Kim, J. Y. Kim, *Nat. Photonics* **2013**, *7*, 732.
[60] R. Aggarwal, D. Saini, S. K. Sonkar, A. K. Sonker, G. Westman, *Chemosphere* **2022**, *287*, 132287.
[61] S. Y. Lim, W. Shen, Z. Gao, *Chem. Soc. Rev.* **2015**, *44*, 362.
[62] C. Rosso, G. Filippini, M. Prato, *ACS Catal.* **2020**, *10*, 8090.
[63] X. Xu, R. Ray, Y. Gu, H. J. Ploehn, L. Gearheart, K. Raker, W. A. Scrivens, *J. Am. Chem. Soc.* **2004**, *126*, 12736.
[64] N. Mohanty, D. Moore, Z. Xu, T. S. Sreeprasad, A. Nagaraja, A. A. Rodriguez, V. Berry, *Nat. Commun.* **2012**, *3*, 844.
[65] J. Peng, W. Gao, B. K. Gupta, Z. Liu, R. Romero-Aburto, L. Ge, L. Song, L. B. Alemany, X. Zhan, G. Gao, *Nano Lett.* **2012**, *12*, 844.
[66] J. Gao, M. Zhu, H. Huang, Y. Liu, Z. Kang, *Inorg. Chem. Front.* **2017**, *4*, 1963.
[67] C. Hu, M. Li, J. Qiu, Y. P. Sun, *Chem. Soc. Rev.* **2019**, *48*, 2315.
[68] S. Y. Park, H. U. Lee, E. S. Park, S. C. Lee, J.-W. Lee, S. W. Jeong, C. H. Kim, Y.-C. Lee, Y. S. Huh, J. Lee, *ACS Appl. Mater. Interfaces* **2014**, *6*, 3365.
[69] Z. Zhu, R. Cheng, L. Ling, Q. Li, S. Chen, *Angew. Chem., Int. Ed.* **2020**, *59*, 3099.
[70] G. A. M. Hutton, B. C. M. Martindale, E. Reisner, *Chem. Soc. Rev.* **2017**, *46*, 6111.
[71] V. Strauss, J. T. Margraf, C. Dolle, B. Butz, T. J. Nacken, J. Walter, W. Bauer, W. Peukert, E. Spiecker, T. Clark, *J. Am. Chem. Soc.* **2014**, *136*, 17308.
[72] F. Arcudi, L. Đorđević, M. Prato, *Angew. Chem.* **2016**, *128*, 2147.
[73] M. Righetto, A. Privitera, I. Fortunati, D. Mosconi, M. Zerbetto, M. L. Curri, M. Corricelli, A. Moretto, S. Agnoli, L. Franco, R. Bozio, C. Ferrante, *J. Phys. Chem. Lett.* **2017**, *8*, 2236.
[74] Y. Song, S. Zhu, S. Zhang, Y. Fu, L. Wang, X. Zhao, B. Yang, *J. Mater. Chem. C* **2015**, *3*, 5976.
[75] M. A. Sk, A. Ananthanarayanan, L. Huang, K. H. Lim, P. Chen, *J. Mater. Chem. C* **2014**, *2*, 6954.
[76] Y. Zhou, E. M. Zahran, B. A. Quiroga, J. Perez, K. J. Mintz, Z. Peng, P. Y. Liyanage, R. R. Pandey, C. C. Chusuei, R. M. Leblanc, *Appl. Catal. B* **2019**, *248*, 157.
[77] K. D. Yang, Y. Ha, U. Sim, J. An, C. W. Lee, K. Jin, Y. Kim, J. Park, J. S. Hong, J. H. Lee, H.-E. Lee, H.-Y. Jeong, H. Kim, K. T. Nam, *Adv. Funct. Mater.* **2016**, *26*, 233.
[78] F. Yuan, T. Yuan, L. Sui, Z. Wang, Z. Xi, Y. Li, X. Li, L. Fan, Z. Tan, A. Chen, M. Jin, S. Yang, *Nat. Commun.* **2018**, *9*, 2249.
[79] J. Zong, Y. Zhu, X. Yang, J. Shen, C. Li, *Chem. Commun.* **2011**, *47*, 764.
[80] S. Atabaev, *Mater. Today: Proc.* **2017**, *4*, 4896.
[81] M. Moniruzzaman, B. A. Lakshmi, S. Kim, J. Kim, *Nanoscale* **2020**, *12*, 11947.
[82] S. H. Lee, D. Y. Kim, J. Lee, S. B. Lee, H. Han, Y. Y. Kim, S. C. Mun, S. H. Im, T. H. Kim, O. O. Park, *Nano Lett.* **2019**, *19*, 5437.
[83] Q. Xu, T. Kuang, Y. Liu, L. Cai, X. Peng, T. S. Sreeprasad, P. Zhao, Z. Yu, N. Li, *J. Mater. Chem. B* **2016**, *4*, 7204.
[84] H. Liu, J. Ding, K. Zhang, L. Ding, *TrAC, Trends Anal. Chem.* **2019**, *118*, 315.
[85] H. Lu, W. Li, H. Dong, M. Wei, *Small* **2019**, *15*, 1902136.
[86] P. Wu, P. Du, H. Zhang, C. Cai, *Phys. Chem. Chem. Phys.* **2013**, *15*, 6920.
[87] S. Zhu, Q. Meng, L. Wang, J. Zhang, Y. Song, H. Jin, K. Zhang, H. Sun, H. Wang, B. Yang, *Angew. Chem.* **2013**, *125*, 4045.
[88] H. Liu, H. Wang, Y. Qian, J. Zhuang, L. Hu, Q. Chen, S. Zhou, *ACS Appl. Nano Mater.* **2019**, *2*, 7043.
[89] T. F. Yeh, C. Y. Teng, S. J. Chen, H. Teng, *Adv. Mater.* **2014**, *26*, 3297.
[90] X. Hai, Q.-X. Mao, W.-J. Wang, X.-F. Wang, X.-W. Chen, J.-H. Wang, *J. Mater. Chem. B* **2015**, *3*, 9109.
[91] P. Gong, J. Wang, K. Hou, Z. Yang, Z. Wang, Z. Liu, X. Han, S. Yang, *Carbon* **2017**, *112*, 63.
[92] Y. Li, H. Lin, C. Luo, Y. Wang, C. Jiang, R. Qi, R. Huang, J. Travas-sejdic, H. Peng, *RSC Adv.* **2017**, *7*, 32225.
[93] Y. Hu, L. Zhang, X. Li, R. Liu, L. Lin, S. Zhao, *ACS Sustainable Chem. Eng.* **2017**, *5*, 4992.
[94] W. Kwon, J. Lim, J. Lee, T. Park, S.-W. Rhee, *J. Mater. Chem. C* **2013**, *1*, 2002.
[95] G. Wang, Q. Guo, D. Chen, Z. Liu, X. Zheng, A. Xu, S. Yang, G. Ding, *ACS Appl. Mater. Interfaces* **2018**, *10*, 5750.
[96] Y. Xu, D. Li, M. Liu, F. Niu, J. Liu, E. Wang, *Sci. Rep.* **2017**, *7*, 4499.
[97] Z. Zhu, P. Yang, X. Li, M. Luo, W. Zhang, M. Chen, X. Zhou, *Spectrochim. Acta, Part A* **2020**, *227*, 117659.
[98] P. Khare, A. Bhati, S. R. Anand, S. K. S. Gunture, *ACS Omega* **2018**, *3*, 5187.
[99] H. Y. Zhang, Y. Wang, S. Xiao, H. Wang, J. H. Wang, L. Feng, *Biosens. Bioelectron.* **2017**, *87*, 46.
[100] S. Qu, D. Shen, X. Liu, P. Jing, L. Zhang, W. Ji, H. Zhao, X. Fan, H. Zhang, *Part. Part. Syst. Charact.* **2014**, *31*, 1175.
[101] C. T. Chien, S. S. Li, W. J. Lai, Y. C. Yeh, H. A. Chen, I. S. Chen, L. C. Chen, K. H. Chen, T. Nemoto, S. Isoda, *Angew. Chem., Int. Ed.* **2012**, *51*, 6662.
[102] Y. Xiong, J. Schneider, C. J. Reckmeier, H. Huang, P. Kasák, A. L. Rogach, *Nanoscale* **2017**, *9*, 11730.
[103] F. Ehrat, S. Bhattacharyya, J. Schneider, A. Löf, R. Wyrwich, A. L. Rogach, J. K. Stolarczyk, A. S. Urban, J. Feldmann, *Nano Lett.* **2017**, *17*, 7710.
[104] E. A. Stepanidenko, I. A. Arefina, P. D. Khavlyuk, A. Dubavik, K. V. Bogdanov, D. P. Bondarenko, S. A. Cherevkov, E. V. Kundelev, A. V. Fedorov, A. V. Baranov, *Nanoscale* **2020**, *12*, 602.
[105] H. Ding, S.-B. Yu, J.-S. Wei, H.-M. Xiong, *ACS Nano* **2016**, *10*, 484.
[106] L. Bao, C. Liu, Z. L. Zhang, D. W. Pang, *Adv. Mater.* **2015**, *27*, 1663.
[107] T.-F. Yeh, W.-L. Huang, C.-J. Chung, I. T. Chiang, L.-C. Chen, H.-Y. Chang, W.-C. Su, C. Cheng, S.-J. Chen, H. Teng, *J. Phys. Chem. Lett.* **2016**, *7*, 2087.

[108] H. Tetsuka, R. Asahi, A. Nagoya, K. Okamoto, I. Tajima, R. Ohta, A. Okamoto, *Adv. Mater.* **2012**, *24*, 5333.
[109] H. Tetsuka, A. Nagoya, T. Fukusumi, T. Matsui, *Adv. Mater.* **2016**, *28*, 4632.
[110] Z. Zhou, E. V. Ushakova, E. Liu, X. Bao, D. Li, D. Zhou, Z. Tan, S. Qu, A. L. Rogach, *Nanoscale* **2020**, *12*, 10987.
[111] S. Hu, R. Tian, Y. Dong, J. Yang, J. Liu, Q. Chang, *Nanoscale* **2013**, *5*, 11665.
[112] L. Li, G. Wu, G. Yang, J. Peng, J. Zhao, J.-J. Zhu, *Nanoscale* **2013**, *5*, 4015.
[113] G. Eda, Y. Y. Lin, C. Mattevi, H. Yamaguchi, H. A. Chen, I. S. Chen, C. W. Chen, M. Chhowalla, *Adv. Mater.* **2010**, *22*, 505.
[114] K. P. Loh, Q. Bao, G. Eda, M. Chhowalla, *Nat. Chem.* **2010**, *2*, 1015.
[115] J. Zhu, H. Shao, X. Bai, Y. Zhai, Y. Zhu, X. Chen, G. Pan, B. Dong, L. Xu, H. Zhang, *Nanotechnology* **2018**, *29*, 245702.
[116] S. Zhu, J. Zhang, X. Liu, B. Li, X. Wang, S. Tang, Q. Meng, Y. Li, C. Shi, R. Hu, *RSC Adv.* **2012**, *2*, 2717.
[117] S. Zhu, J. Zhang, S. Tang, C. Qiao, L. Wang, H. Wang, X. Liu, B. Li, Y. Li, W. Yu, X. Wang, H. Sun, Y. Bai, *Adv. Funct. Mater.* **2012**, *22*, 4732.
[118] T. K. Henna, K. Pramod, *Mater. Sci. Eng., C* **2020**, *110*, 110651.
[119] L. Li, T. Dong, *J. Mater. Chem. C* **2018**, *6*, 7944.
[120] S. Cong, Z. Zhao, *Carbon Quantum Dots: A Component of Efficient Visible Light Photocatalysts*, InTechOpen, London **2018**.
[121] Q. Xue, H. Huang, L. Wang, Z. Chen, M. Wu, Z. Li, D. Pan, *Nanoscale* **2013**, *5*, 12098.
[122] X. Teng, C. Ma, C. Ge, M. Yan, J. Yang, Y. Zhang, P. C. Morais, H. Bi, *J. Mater. Chem. B* **2014**, *2*, 4631.
[123] L. Wu, M. Luderer, X. Yang, C. Swain, H. Zhang, K. Nelson, A. J. Stacy, B. Shen, G. M. Lanza, D. Pan, *Theranostics* **2013**, *3*, 677.
[124] V. Kumar, K.-H. Kim, P. Kumar, B.-H. Jeon, J.-C. Kim, *Coord. Chem. Rev.* **2017**, *342*, 80.
[125] J. Jana, M. Ganguly, B. Das, S. Dhara, Y. Negishi, T. Pal, *Talanta* **2016**, *150*, 253.
[126] P. Das, S. Ganguly, S. Mondal, M. Bose, A. K. Das, S. Banerjee, N. C. Das, *Sens. Actuators, B* **2018**, *266*, 583.
[127] M. M. Doroodmand, M. Askari, *Anal. Chim. Acta* **2017**, *968*, 74.
[128] B. P. Jiang, B. Zhou, X. C. Shen, Y. X. Yu, S. C. Ji, C. C. Wen, H. Liang, *Chemistry* **2015**, *21*, 18993.
[129] B. Wu, G. Zhu, A. Dufresne, N. Lin, *ACS Appl. Mater. Interfaces* **2019**, *11*, 16048.
[130] Y. Qin, J. Lu, S. Li, Z. Li, S. Zheng, *J. Phys. Chem. C* **2014**, *118*, 20538.
[131] N. Stevens, D. L. Akins, *Sens. Actuators, B* **2007**, *123*, 59.
[132] X. Sun, Y. Lei, *TrAC, Trends Anal. Chem.* **2017**, *89*, 163.
[133] M. Ganiga, J. Cyriac, *Sens. Actuators, B* **2016**, *225*, 522.
[134] Y. Liu, W. Li, P. Wu, C. Ma, X. Wu, M. Xu, S. Luo, Z. Xu, S. Liu, *Sens. Actuators, B* **2019**, *281*, 34.
[135] R. Zhang, Y. Liu, L. Yu, Z. Li, S. Sun, *Nanotechnology* **2013**, *24*, 225601.
[136] X. Shan, L. Chai, J. Ma, Z. Qian, J. Chen, H. Feng, *Analyst* **2014**, *139*, 2322.
[137] G. Liu, H. Ge, R. Yin, L. Yu, C. Sun, W. Dong, Z. Sun, K. A. Alamry, H. M. Marwani, S. Wang, *Anal. Methods* **2020**, *12*, 1617.
[138] Y. Shan, Y. Liu, Y. Li, W. Yang, *Sep. Purif. Technol.* **2020**, *250*, 117181.
[139] N. S. Lawrence, L. Jiang, T. G. J. Jones, R. G. Compton, *Anal. Chem.* **2003**, *75*, 2054.
[140] L. Ferrer, G. de Armas, M. Miró, J. M. Estela, V. c. Cerdà, *Talanta* **2004**, *64*, 1119.
[141] A. Sola, A. Tárraga, P. Molina, *Org. Biomol. Chem.* **2014**, *12*, 2547.
[142] Y. Xu, H. Yu, L. Chudal, N. K. Pandey, E. H. Amador, B. Bui, L. Wang, X. Ma, S. Deng, X. Zhu, S. Wang, W. Chen, *Mater. Today Phys.* **2021**, *17*, 100328.
[143] N. Thongsai, P. Jaiyong, S. Kladsomboon, I. In, P. Paoprasert, *Appl. Surf. Sci.* **2019**, *487*, 1233.
[144] A. K. Goyal, H. S. Dutta, S. Pal, *J. Phys. D: Appl. Phys.* **2017**, *50*, 203001.
[145] G. Huang, Y. Li, C. Chen, Z. Yue, W. Zhai, M. Li, B. Yang, *J. Phys. D: Appl. Phys.* **2020**, *53*, 325102.
[146] A. Mhamdi, M. S. Alkhalifah, S. Rajeh, A. Labidi, M. Amlouk, S. Belgacem, *Phys. B* **2017**, *521*, 178.
[147] M. Carminati, *J. Sens.* **2017**, *2017*, 7638389.
[148] R. S. Andre, R. C. Sanfelice, A. Pavinatto, L. H. C. Mattoso, D. S. Correa, *Mater. Des.* **2018**, *156*, 154.
[149] W. Chen, F. Li, P. C. Ooi, Y. Ye, T. W. Kim, T. Guo, *Sens. Actuators, B* **2016**, *222*, 763.
[150] M. Ghazi, S. Janfaza, H. Tahmooressi, A. Ravishankara, E. Earl, N. Tasnim, M. Hoorfar, *Sens. Actuators, B* **2021**, *342*, 130050.
[151] J. Hu, C. Zou, Y. Su, M. Li, N. Hu, H. Ni, Z. Yang, Y. Zhang, *J. Mater. Chem. C* **2017**, *5*, 6862.
[152] S. Shao, H. W. Kim, S. S. Kim, Y. Chen, M. Lai, *Appl. Surf. Sci.* **2020**, *516*, 145932.
[153] N. Lim, J.-S. Lee, Y. T. Byun, *Nanomaterials* **2020**, *10*, 2509.
[154] Y. Zou, S. Chen, J. Sun, J. Liu, Y. Che, X. Liu, J. Zhang, D. Yang, *ACS Sens.* **2017**, *2*, 897.
[155] X. Wang, J. Su, H. Chen, G.-D. Li, Z. Shi, H. Zou, X. Zou, *ACS Appl. Mater. Interfaces* **2017**, *9*, 16335.
[156] G.-J. Sun, J. K. Lee, S. Choi, W. I. Lee, H. W. Kim, C. Lee, *ACS Appl. Mater. Interfaces* **2017**, *9*, 9975.
[157] Y.-M. Long, L. Bao, Y. Peng, Z.-L. Zhang, D.-W. Pang, *Carbon* **2018**, *129*, 168.
[158] Y.-K. Lv, Y.-Y. Li, H.-C. Yao, Z.-J. Li, *Sens. Actuators, B* **2021**, *339*, 129882.
[159] X. Lai, D. Wang, N. Han, J. Du, J. Li, C. Xing, Y. Chen, X. Li, *Chem. Mater.* **2010**, *22*, 3033.
[160] J.-L. Wang, Q.-G. Zhai, S.-N. Li, Y.-C. Jiang, M.-C. Hu, *Inorg. Chem. Commun.* **2016**, *63*, 48.
[161] Q. Yang, Y. Wang, J. Liu, J. Liu, Y. Gao, P. Sun, J. Zheng, T. Zhang, Y. Wang, G. Lu, *Sens. Actuators, B* **2017**, *241*, 806.
[162] D. R. Miller, S. A. Akbar, P. A. Morris, *Sens. Actuators, B* **2014**, *204*, 250.
[163] Y.-K. Lv, Y.-Y. Li, R.-H. Zhou, Y.-P. Pan, H.-C. Yao, Z.-J. Li, *ACS Appl. Mater. Interfaces* **2020**, *12*, 34245.
[164] M. Cheng, Z. Wu, G. Liu, L. Zhao, Y. Gao, S. Li, B. Zhang, X. Yan, G. Lu, *Sens. Actuators, B* **2020**, *304*, 127272.
[165] S. Shao, X. Chen, Y. Chen, L. Zhang, H. W. Kim, S. S. Kim, *ACS Appl. Nano Mater.* **2020**, *3*, 5220.
[166] S. Shao, W. Wang, K. Zhou, F. Jiang, H. Wu, R. Koehn, *Mater. Lett.* **2017**, *186*, 193.
[167] L. Al-Mashat, K. Shin, K. Kalantar-Zadeh, J. D. Plessis, S. H. Han, R. W. Kojima, R. B. Kaner, D. Li, X. Gou, S. J. Ippolito, *J. Phys. Chem. C* **2010**, *114*, 16168.
[168] J. N. Gavgani, A. Hasani, M. Nouri, M. Mahyari, A. Salehi, *Sens. Actuators, B* **2016**, *229*, 239.
[169] Y. Zhang, J. Zhao, H. Sun, Z. Zhu, J. Zhang, Q. Liu, *Sens. Actuators, B* **2018**, *266*, 364.
[170] T. Y. Li, C. Y. Duan, Y. X. Zhu, Y. F. Chen, Y. Wang, *J. Phys. D: Appl. Phys.* **2017**, *50*, 114002.
[171] R. Wang, G. Li, Y. Dong, Y. Chi, G. Chen, *Anal. Chem.* **2013**, *85*, 8065.
[172] Y. Wang, H. Meng, M. Jia, Y. Zhang, H. Li, L. Feng, *Nanoscale* **2016**, *8*, 17190.
[173] M. Zheng, Y. Li, Y. Zhang, Z. Xie, *RSC Adv.* **2016**, *6*, 83501.
[174] S. Dolai, S. K. Bhunia, R. Jelinek, *Sens. Actuators, B* **2017**, *241*, 607.
[175] N. A. Travlou, J. Secor, T. J. Bandosz, *Carbon* **2017**, *114*, 544.
[176] C. Wang, Y. Ding, X. Bi, J. Luo, G. Wang, Y. Lin, *Sens. Actuators, B* **2018**, *264*, 404.
[177] M. Wang, Y. Xia, J. Qiu, X. Ren, *Spectrochim. Acta, Part A* **2019**, *206*, 170.
[178] R. Parvizi, S. Azad, K. Dashtian, M. Ghaedi, H. Heidari, *Sci. Rep.* **2019**, *9*, 3798.

[179] P. Supchocksoonthorn, N. Thongsai, H. Moonmuang, S. Kladsomboon, P. Jaiyong, P. Paoprasert, *Colloids Surf., A* **2019**, *575*, 118.
[180] J. N. Gavgani, H. S. Dehsari, A. Hasani, M. Mahyari, E. K. Shalamzari, A. Salehi, F. A. Taromi, *RSC Adv.* **2015**, *5*, 57559.
[181] S. Shao, Y. Chen, S. Huang, F. Jiang, Y. Wang, R. Koehn, *RSC Adv.* **2017**, *7*, 39859.
[182] Y.-H. Zhang, C.-N. Wang, L.-J. Yue, J.-L. Chen, F.-L. Gong, S.-M. Fang, *Phys. E* **2021**, *133*, 114807.
[183] W. Wu, C. Jiang, V. A. L. Roy, *Nanoscale* **2015**, *7*, 38.
[184] J. Lyu, J. Gao, M. Zhang, Q. Fu, L. Sun, S. Hu, J. Zhong, S. Wang, J. Li, *Appl. Catal. B* **2017**, *202*, 664.
[185] A. M. Alansi, M. Al-Qunaibit, I. O. Alade, T. F. Qahtan, T. A. Saleh, *J. Mol. Liq.* **2018**, *253*, 297.
[186] A. M. Alansi, T. F. Qahtan, T. A. Saleh, *Adv. Mater. Interfaces* **2020**, *8*, 2001463.
[187] A. M. Alansi, T. F. Qahtan, N. Al Abass, J. M. AlGhamdi, M. Al-Qunaibit, T. A. Saleh, *Adv. Sustainable Syst.* **2021**, *6*, 2100267.
[188] B. Bajorowicz, M. P. Kobylański, A. Gołąbiewska, J. Nadolna, A. Zaleska-Medynska, A. Malankowska, *Adv. Colloid Interface Sci.* **2018**, *256*, 352.
[189] E. G. Alvarez, H. Wortham, R. Strekowski, C. Zetzsch, S. X. Gligorovski, *Environ. Sci. Technol.* **2012**, *46*, 1955.
[190] H. Yu, Q. Zhu, Z. Tan, *Appl. Energy* **2012**, *93*, 53.
[191] T. Tanaka, K. Teramura, K. Arakaki, T. Funabiki, *Chem. Commun.* **2002**, 2742.
[192] N. Macleod, R. Cropley, J. M. Keel, R. M. Lambert, *J. Catal.* **2004**, *221*, 20.
[193] P. Granger, V. I. Parvulescu, *Chem. Rev.* **2011**, *111*, 3155.
[194] J. Lasek, Y.-H. Yu, J. C. S. Wu, *J. Photochem. Photobiol., C* **2013**, *14*, 29.
[195] Y. Liu, S. Yu, Z. Zhao, F. Dong, X. A. Dong, Y. Zhou, *J. Phys. Chem. C* **2017**, *121*, 12168.
[196] Y. Cui, T. Wang, J. Liu, L. Hu, Q. Nie, Z. Tan, H. Yu, *Chem. Eng. J.* **2021**, *420*, 129595.
[197] Y. Huang, Y. Liang, Y. Rao, D. Zhu, J.-j. Cao, Z. Shen, W. Ho, S. C. Lee, *Environ. Sci. Technol.* **2017**, *51*, 2924.
[198] Y. Lu, Y. Huang, J.-j. Cao, H. Li, W. Ho, S. C. Lee, *J. Mater. Chem. A* **2019**, *7*, 15782.
[199] X. Li, H. Shi, X. Yan, S. Zuo, Y. Zhang, T. Wang, S. Luo, C. Yao, C. Ni, *ACS Sustainable Chem. Eng.* **2018**, *6*, 10616.
[200] R. Sun, Q. Shi, M. Zhang, L. Xie, J. Chen, X. Yang, M. Chen, W. Zhao, *J. Alloys Compd.* **2017**, *714*, 619.
[201] X. a. Dong, W. Cui, H. Wang, J. Li, Y. Sun, H. Wang, Y. Zhang, H. Huang, F. Dong, *Sci. Bull.* **2019**, *64*, 669.
[202] W. Cui, J. Li, L. Chen, X. a. Dong, H. Wang, J. Sheng, Y. Sun, Y. Zhou, F. Dong, *Sci. Bull.* **2020**, *65*, 1626.
[203] M. J. Aminoff, S. A. Josephson, *Aminoff's Neurology and General Medicine*, Elsevier, Oxford **2014**.
[204] H. Zhang, H. Ming, S. Lian, H. Huang, H. Li, L. Zhang, Y. Liu, Z. Kang, S. T. Lee, *Dalton Trans.* **2011**, *40*, 10822.
[205] Y. Liu, C. Zhu, J. Sun, Y. Ge, F. Song, Q. Xu, *New J. Chem.* **2020**, *44*, 3455.
[206] G. Huang, L. Liu, L. Chen, L. Gao, J. Zhu, H. Fu, *J. Hazard. Mater.* **2021**, *423*, 127134.
[207] E. Uhde, T. Salthammer, *Atmos. Environ.* **2007**, *41*, 3111.
[208] Y. Hu, X. Xie, X. Wang, Y. Wang, Y. Zeng, D. Y. H. Pui, J. Sun, *Appl. Surf. Sci.* **2018**, *440*, 266.
[209] X. Qian, D. Yue, Z. Tian, M. Reng, Y. Zhu, M. Kan, T. Zhang, Y. Zhao, *Appl. Catal. B* **2016**, *193*, 16.
[210] M. Riva, E. S. Robinson, E. Perraudin, N. M. Donahue, E. Villenave, *Environ. Sci. Technol.* **2015**, *49*, 5407.
[211] H. O. T. Pye, G. A. Pouliot, *Environ. Sci. Technol.* **2012**, *46*, 6041.
[212] J. S. Gaffney, N. A. Marley, *Atmos. Environ.* **2009**, *43*, 23.
[213] M. Takeuchi, M. Hidaka, M. Anpo, *J. Hazard. Mater.* **2012**, *237*, 133.
[214] J. Yu, A. Caravaca, C. Guillard, P. Vernoux, L. Zhou, L. Wang, J. Lei, J. Zhang, Y. Liu, *Catalysts* **2021**, *11*, 464.
[215] X. Zhao, B. Deng, F. Li, M. Huang, Y. Sun, J. Li, F. Dong, *J. Hazard. Mater.* **2021**, *420*, 126577.
[216] M. Wang, J. Hua, Y. Yang, *Spectrochim. Acta, Part A* **2018**, *199*, 102.
[217] K. Li, Y. He, J. Li, J. Sheng, Y. Sun, J. Li, F. Dong, *J. Hazard. Mater.* **2021**, *416*, 126208.
[218] C. He, P. Li, J. Cheng, Z.-P. Hao, Z.-P. Xu, *Water, Air, Soil Pollut.* **2010**, *209*, 365.
[219] H. Wu, L. Wang, J. Zhang, Z. Shen, J. Zhao, *Catal. Commun.* **2011**, *12*, 859.
[220] S. Kashiwaya, T. Toupance, A. Klein, W. Jaegermann, *Adv. Energy Mater.* **2018**, *8*, 1802195.
[221] A. Mahmood, X. Wang, G. Shi, Z. Wang, X. Xie, J. Sun, *J. Hazard. Mater.* **2020**, *386*, 121962.
[222] A. Mahmood, G. Shi, Z. Wang, Z. Rao, W. Xiao, X. Xie, J. Sun, *J. Hazard. Mater.* **2021**, *401*, 123402.
[223] S. R. Kim, W. K. Jo, *J. Hazard. Mater.* **2019**, *380*, 120866.
[224] Q. Dai, S. Bai, J. Wang, M. Li, X. Wang, G. Lu, *Appl. Catal., B* **2013**, *142*, 222.
[225] F. Zhang, X. Li, Q. Zhao, D. Zhang, *ACS Sustainable Chem. Eng.* **2016**, *4*, 4554.
[226] J. Li, X. Li, L. Zeng, S. Fan, M. Zhang, W. Sun, X. Chen, M. O. Tade, S. Liu, *Nanoscale* **2019**, *11*, 3877.
[227] J. Ding, H. Wang, Y. Luo, Y. Xu, J. Liu, R. Lin, Y. Gao, Y. Lin, *Nanomaterials* **2020**, *10*, 1795.
[228] Y. Liu, C. Zhu, J. Sun, Y. Ge, F. Song, G. Wang, Q. Xu, *Environ. Sci. Pollut. Res.* **2021**, *28*, 25949.
[229] Y. Huang, Y. Gao, Q. Zhang, Y. Zhang, J. J. Cao, W. Ho, S. C. Lee, *J. Hazard. Mater.* **2018**, *354*, 54.
[230] Y. Xie, S. Yu, Y. Zhong, Q. Zhang, Y. Zhou, *Appl. Surf. Sci.* **2018**, *448*, 655.
[231] N. C. T. Martins, J. Angelo, A. V. Girao, T. Trindade, L. Andrade, A. Mendes, *Appl. Catal. B* **2016**, *193*, 67.
[232] J. Wang, F. Han, Y. Rao, T. Hu, Y. Huang, J.-j. Cao, S. C. Lee, *Ind. Eng. Chem. Res.* **2018**, *57*, 10226.
[233] J. Qin, R. Zhao, M. Xia, *Atmos. Pollut. Res.* **2020**, *11*, 303.
[234] Y. Duan, L. Deng, Z. Shi, X. Liu, H. Zeng, H. Zhang, J. Crittenden, *J. Colloid Interface Sci.* **2020**, *561*, 696.

Jungang Zhao received his bachelor's degree in Chemical Engineering and Technology from Taiyuan Institute of Technology in 2013. He is now a Ph.D. student in the School of Environmental Science and Engineering at Hunan University, majoring in air pollutant control under the supervision of Prof. Caiting Li. His current research interests are focused on the design and synthesis of photothermal catalysts for energy and environmental applications.

Caiting Li received his Ph.D. degree at Hunan University. He is a Professor and Supervisor of doctoral students of Hunan University. His research interests focus on air pollution control, including dedusting, desulfurization, DeNOx, mercury removal, and VOCs pollution control. He has conducted and carried out more than 30 national and provincial research projects. He has published over 150 papers and has over 19 patents in the field of air pollution control.